Reduced-order methods for dynamic problems in topology optimization: A comparative study

Li, Quhao; Sigmund, Ole; Jensen, Jakob Søndergaard; Aage, Niels

Published in:
Computer Methods in Applied Mechanics and Engineering

Link to article, DOI:
10.1016/j.cma.2021.114149

Publication date:
2021

Document Version
Peer reviewed version

Reduced-order methods for dynamic problems in topology optimization: a comparative study

Quhao Li [a,1], Ole Sigmund [b], Jakob Søndergaard Jensen [b], Niels Aage [b]

[a] *Key Laboratory of High Efficiency and Clean Mechanical Manufacture of MOE, School of Mechanical Engineering, Shandong University, Jinan 250061, PR China*
[b] *Department of Mechanical Engineering, Solid Mechanics, Technical University of Denmark, 2800 Kgs. Lyngby, Denmark*

Abstract

The dynamics of engineering structures are of great importance for topology optimization problems in both academia and industry. However, for design problems where broadband frequency responses are required, the computational burden becomes enormous, especially for large-scale applications. To remedy this numerical bottleneck, using the Reduced-Order Methods (ROMs) is an efficient approach by recasting the original problem into a subspace with a much smaller dimensionality than the full model. In this paper, a systematic comparative study of some typical and potential ROMs for solving the broadband frequency response optimization problems is provided, including the Quasi-Static Ritz Vector (QSRV), the Padé expansion and the second-order Krylov subspace method. Furthermore, the effects of the orthonormalization processes are discussed. Two representative test problems, a vibration problem and a wave propagation problem, are solved, analyzed, and compared based on the ROMs' accuracy, their stability in approximating the state and adjoint equations and the applicability to topology optimization problems. From the extensive numerical results, we find that the second-order Krylov subspace with moment-matching Gram-Schmidt orthonormalization (SOMMG) and the Second-Order Arnoldi method (SOAR) provides superior accuracy and stability. Moreover, the results verify that the basis vectors computed for the state equation cannot be reused for solving the adjoint equation, and hence, that new basis vectors should be constructed. Analysis of the computational cost for the 3D test problems show an improvement in numerical performance in the order of 100-10000 for the ROMs compared to the full approach.

Keywords: Reduced-order methods; Frequency response; Topology optimization; Quasi-static Ritz vector method; Padé expansion; Second-order Krylov subspace method

1 Introduction

Dynamics and harmonic vibrations play a crucial role in the performance of many engineering structures ranging from large-scale structures, e.g. aircrafts and bridges, to microdevices such as MEMS inertial sensors. In most cases, reducing the vibration amplitude is preferred for improving the comfort level, noise reduction, avoiding feedback loops, or prolonging service time. On the other

[1] Corresponding author.
E-mail address: quhaoli@sdu.edu.cn.

hand, some devices utilize resonance phenomena to sustain large vibration amplitudes, such as high precision sensors [1] or energy harvesters [2]. Designing vibrating components or structures for different applications has been a hot topic, both in engineering and academia. In recent years, structural optimization has come to play a more and more important role in the pursuit of improving structural characteristics by systematic utilization of the finite element procedure and optimization methods. According to the types of design variables, structural optimization falls into three categories: size optimization, shape optimization, and topology optimization. Of these, topology optimization is the one with the largest potential for generating excellent and innovative designs without excessive dependency on engineering experience. Over the past 30 years, several topology optimization methods have been developed, including homogenization based methods [3], density-based methods [4,5], level set methods [6,7], evolutionary methods [8], and component-based methods [9,10].

The first work of topology optimization for dynamic problems can be traced back to the study by Díaaz and Kikuchi [11], in which the structural natural frequency is maximized using the homogenization based method. Subsequently, numerous works on eigenvalue based topology optimization have been carried out, including maximizing the natural frequency [12], band-gap maximization [13] and frequency band constraints [14]. Another important research direction is to improve the dynamic response under external loads, such as structural displacements, velocities, accelerations, and stresses, in the time domain [15-17] or the frequency domain [18-20]. This approach can lead to novel solutions for specific functional demands. For example, in the frequency domain, Tcherniak et al. [21] optimized the layout of resonating actuators to maximize the magnitude of steady-state vibrations for a given excitation frequency. Larsen et al. [22] designed elastic plates for vibration suppression and guided transport of vibrational energy. Sigmund and Jensen [23] studied the design of phononic band-gap materials and structures using topology optimization. In the time domain, Matzen et al. [24] developed a topology optimization scheme for the transient response of photonic crystal structures. Nakshatrala et al. [25] proposed a design method for effective energy propagation with elastoplastic material behavior.

Although topology optimization has been widely employed for dynamic design problems, the computational cost is still a limiting factor for practical engineering applications. In natural frequency design problems, only a limited number of low-order eigenfrequencies have been considered due to the cost of solving the underlying eigenvalue problem. For the harmonic or transient response, the frequency, or temporal intervals, are often discretized by coarse steps and/or over small ranges. Considering more eigenfrequencies, or smaller time or frequency steps, require vast amounts of computational resources and time in order to solve the linear equations arising in the finite element analysis. Furthermore, practical applications often require high-resolution spatial discretization of the governing partial differential equations to ensure an accurate solution at the highest angular frequency. This is needed in order to avoid numerical dispersion and results in very large-scale matrices in the finite element model. It is well known that the majority of the computational cost involved in structural optimization problems is associated with the repetitive solution of the state equations and adjoint equations. Consequently, it is urgent for researchers to develop highly efficient strategies for the solution of the dynamic equations of motion.

Researchers have proposed several efficient multilevel techniques [26-29] to solve large-scale static optimization problems, leading to topology optimized designs of aircraft wings and suspension bridges with giga-voxel resolution [30,31]. Ferrari [32] proposed to use a frequency response to replace the fundamental eigenvalue problem, and multilevel approaches can be used to solve design problems in the low frequency space efficiently. Recently, a multilevel approach to linearized buckling criteria was developed [33]. However, directly applying these techniques is not always possible in the frequency domain due to the indefiniteness of the linear systems when evaluated above the first eigenfrequency, and more generally, such approaches are prohibited because of the

large number of solutions needed for broad frequency ranges or fine temporal discretization. A more general and efficient approach to remedy this numerical bottleneck is to use Reduced-Order Methods (ROMs) to recast the original problem into a subspace with a much smaller dimensionality than the full model. If the reduction method is efficient, an approximate, yet sufficiently accurate solution, can be obtained with great savings in computational effort and time.

One of the most widely used ROMs is the Modal Superposition Method (MSM), which can be used to approximate both frequency and transient responses of a structure. By using this method, the original problem is projected onto a truncated modal space, and a reduced-order model is obtained for fast frequency sweeps or transient analysis. Ma et al. [34] applied the Modal Displacement Method (MDM) to topology optimization for reducing the computational cost. The number of modal vectors included in the subspace normally determines the accuracy of MSM type strategies. However, for high-frequency responses, the convergence of the method can be quite slow. Cornwell et al. [35] partly remedied this problem by introducing a pseudo-static solution to the reduced bases, thus leading to the Modal Acceleration Method (MAM). In Liu et al. [36], the authors presented a comparative study of the MDM and the MAM for structural topology optimization under harmonic force excitations. Results showed that the MAM consistently yielded better results than the MDM. Recently, hybrid expansion methods [37,38], which are based on modal superposition and power series expansion of the high-order modes, were introduced for topology optimization problems in order to increase computational accuracy and stability. Nevertheless, all eigenvector-based ROMs suffer from the following limitations: (1) only low-frequency problems can be considered. That is, the effectiveness for mid- or high-frequency problems has not been verified; (2) for a large frequency range, the numerical efficiency will be reduced as large sets of eigenvectors are needed to span the subspace; (3) these methods are suitable for proportionally damped systems, while for the non-proportional damping problem, complex modes should be employed [39]; (4) the computational cost associated with solving the eigenvalue problem itself is prohibitive for application to large-scale systems [40].

An alternative computational technique is to approximate the solution of a dynamic system by a series expansion. Here, the expansion parameters are determined according to the solutions of the system at just a few frequencies. This type of method is also called the moment-matching method. Jensen [41] employed the Padé expansion to represent the frequency response over a given frequency interval, and the analytical sensitivity analysis was derived for density-based topology optimization. However, this method can only provide an accurate approximation of the frequency response over narrow frequency ranges due to insufficient numerical precision caused by ill-conditioned matrices arising when using a large number of expansion terms. This is also verified in the present work by the numerical results in section 4.2.1. The Ritz Vector method (RV) is an alternative non-modal expansion technique and Yoon [42] compared the RV, the Quasi-Static Ritz Vector (QSRV) and the standard Modal Displacement Method (MDM) for use in topology optimization. It was shown that the QSRV method can be used as an alternative ROM scheme and that it leads to a stable optimization process. Similar to the QSRV is the family of Krylov subspace methods [43,44], which forms the basis for many ROMs. These are, for example, often used for the solution of large-scale linear systems and eigenvalue problems. For most dynamic problems, the systems are second-order, and as a consequence, the second-order Krylov subspace method was developed. It has successfully been applied to frequency space analysis of large-scale structures[45], acoustic systems[45,46], etc., but not in the context of topology optimization.

In this work, we provide a systematic comparative study of the QSRV method, the Padé expansion, and the second-order Krylov subspace method for solving wide-band frequency response optimization problems. These methods have been chosen because they possess the biggest potential, and the presented study concerns the solutions of both state and adjoint equations. The latter is of

special interest since previous works lack discussions on the accuracy of a given ROM basis obtained from the forward problem when applied to the adjoint equation. Furthermore, three orthonormalization processes for the second-order Krylov subspace method are tested and their impact on stability and convergence are discussed. The numerical examples consist of two different test problems that are deemed representative of the majority of dynamic topology optimization design problems. The first concerns the minimization of the vibration amplitude of a vibrating beam, whereas the second example deals with maximizing wave propagation through a plate. Both test problems are solved, analyzed, and compared based on a full model solution and solutions based on the different ROMs. Based on our extensive numerical results, we find that the second-order Krylov subspace with moment-matching Gram-Schmidt orthonormalization (SOMMG) and the Second-Order Arnoldi method (SOAR) provides superior accuracy and stability for solving both state and adjoint equations.

The rest of this paper's organization is as follows. Section 2 presents the model equations of motion, i.e., the state equation and the adjoint equation. This is followed by a detailed presentation of the ROMs as pseudocode in Section 3. Section 4 provides the results of the two numerical examples, including comparisons and intermediate conclusions. Finally, a summary and advice for future use are given.

2 Model finite element problem

This section briefly reviews the finite element formulation of the linear dynamic problem in frequency space and introduces the sensitivity analysis and adjoint equation for the considered objective function.

2.1 State equation for linear dynamics

For a general linear dynamic problem, the finite element formulation can be written as follows in the time domain.

$$\mathbf{M}\ddot{\mathbf{u}}(t)+\mathbf{C}\dot{\mathbf{u}}(t)+\mathbf{K}\mathbf{u}(t)=\mathbf{f}(t) \tag{1}$$

where $\mathbf{K}$, $\mathbf{C}$ and $\mathbf{M}$ denote the standard global stiffness, damping, and mass matrices, respectively, and $\mathbf{u}(t)$ and $\mathbf{f}(t)$ are the time-dependent displacement and force vectors [47]. The dot denotes differentiation with respect to time, and hence $\dot{\mathbf{u}}(t)$ and $\ddot{\mathbf{u}}(t)$ represent velocity and acceleration vectors, respectively. Assuming the structure is subjected to a time-harmonic external force $\mathbf{f}(t)=\mathrm{Re}\left(\mathbf{F}e^{i\omega t}\right)$, the equation of motion can be cast in the frequency space by substituting the solution $\mathbf{u}(t)=\mathrm{Re}\left(\mathbf{U}(\omega)e^{i\omega t}\right)$ into equation (1):

$$\left(-\omega^2\mathbf{M}+i\omega\mathbf{C}+\mathbf{K}\right)\mathbf{U}(\omega)=\mathbf{F} \tag{2}$$

where Re( ) represents the real part of a complex number, $\mathbf{U}(\omega)$ is the complex amplitude vector, $\omega\in[\omega_L,\omega_R]$ is the excitation frequency in radians with ω_L and ω_R representing the bounds on the frequency range of interest and i is the imaginary number satisfying $i^2=-1$. For convenience, we define the frequency dependent system matrix as

$$\mathbf{S}(\omega)=\mathbf{K}+i\omega\mathbf{C}\text{-}\omega^2\mathbf{M} \tag{3}$$

and the state equation (2) can be written in compact form as

$$\mathbf{S}(\omega)\mathbf{U}(\omega)=\mathbf{F} \tag{4}$$

Due to the frequency dependent system matrix, this system has to be assembled and solved in a discrete number of frequencies in the interval $\omega\in[\omega_L,\omega_R]$. Most often, it is desirable to have as fine a frequency discretization as possible, and hence, finding an adequate solution over the complete frequency band poses a significant computational burden.

Although this work is focused on the frequency dependent system in the equation (4), we briefly remark that implicit time stepping schemes, such as the popular Newmark algorithm, also involves the repeated solution of a linear system of equations. This may seem similar to that of equation (4), but with the important difference that the resulting system matrix is $\widetilde{\mathbf{K}}\mathbf{U}^{i+1}=\mathbf{F}^{i+1}$. Here i represents the time, and the left term $\widetilde{\mathbf{K}}$ is positive definite and remains constant throughout the time series. Hence, for small-scale problems, the matrix can be factorized once and reused between time steps. For very large-scale problems, the multilevel methods discussed in the introduction can be applied as well. However, the computational burden of the time-stepping schemes may still prohibit their use for structural optimization problems, and hence ROMs are also widely used [48,49] for this class of problems. Some strategies, i.e., using the FFT, can be used to choose the expansion points for such transient problems. Finally, we remark that the ROMs presented and discussed in this work are tailored for frequency-based analysis and that ROMs for transient analysis are outside the scope of this work.

2.2 Model optimization problem

A large number of objective functions for harmonic optimization problems have been studied in previous works, as reviewed in Ref. [50]. In this paper, a generic yet representative optimization problem is considered, corresponding to minimizing or maximizing the vibration magnitude at a predefined line or area. The optimization formulation follows as:

$$\begin{aligned}
&\min_{\rho_e}/\max \quad J=\left(\sum_i^{N_f}\log_{10}(J_i)\right), \qquad J_i=\frac{\left|\mathbf{U}(\omega_i)^{\mathrm{H}}\,\mathbf{L}\mathbf{U}(\omega_i)\right|}{N_l}\\
&s.t. \qquad \sum_{e=1}^{N_e}\bar{\tilde{\rho}}_e v_e \Big/ V-V^*\le 0\\
&\qquad\quad \mathbf{S}(\bar{\tilde{\rho}}_e,\omega_i)\mathbf{U}(\omega_i)=\mathbf{F}, \quad (i=1,\ldots,\ N_f)\\
&\qquad\quad 0\le\rho_e\le 1, \quad (e=1,\ldots,\ N_e)
\end{aligned} \tag{5}$$

where N_f is the number of discrete frequency points in the frequency interval. $\mathbf{L}$ is a zero matrix with ones at the diagonal elements corresponding to the degrees of freedom on the line or area to be minimized/maximized, and N_l represents the number of non-zero elements. Superscript H represents the Hermite transposition, ρ_e is the design variable and N_e represents the number of elements within the design domain. The volume constraint is imposed in this formulation, in which v_e is the volume of the element and V^* is the target volume fraction. In this paper, two materials are considered, and the modified SIMP interpolation [51] is applied:

$$\mathbf{K}_e(\bar{\tilde{\rho}}_e)=\bar{\tilde{\rho}}_e^{\,r}\mathbf{K}_e^{*1}+(1-\bar{\tilde{\rho}}_e^{\,r})\mathbf{K}_e^{*2} \tag{6}$$

$$\mathbf{M}_e(\bar{\tilde{\rho}}_e)=\bar{\tilde{\rho}}_e^{\,q}\mathbf{M}_e^{*1}+(1-\bar{\tilde{\rho}}_e^{\,q})\mathbf{M}_e^{*2} \tag{7}$$

where $\mathbf{K}_e^{*1}$ and $\mathbf{K}_e^{*2}$ are the element stiffness matrices corresponding to the two given solid materials, while $\mathbf{M}_e^{*1}$ and $\mathbf{M}_e^{*2}$ are the element mass matrices and r and q are the penalization factors. The design problem is regularized using a projection filter such that the physical density $\bar{\tilde{\rho}}_e$ is computed by [52]:

$$\bar{\tilde{\rho}}_e = \frac{\tanh(\beta\eta) + \tanh\left(\beta\left(\tilde{\rho}_e - \eta\right)\right)}{\tanh(\beta\eta) + \tanh\left(\beta\left(1-\eta\right)\right)} \tag{8}$$

where β determines the steepness of the projection and η is the threshold value. The smoothed design variable $\tilde{\rho}_e$ is obtained through a convolution type density filter, i.e.

$$\tilde{\rho}_e = \frac{\sum_{j\in\Xi_e} w(\mathbf{x}_j) v_j \rho_j}{\sum_{j\in\Xi_e} w(\mathbf{x}_j) v_j} \tag{9}$$

where ρ_j and v_j represent the mathematical design variable and the volume of the j^{th} element, respectively. The linear weight factors are given by $w(\mathbf{x}_j) = r_{\min} - \|\mathbf{x}_j - \mathbf{x}_e\|$ where $\mathbf{x}_j$ is the coordinate of the j^{th} element center, $\|\bullet\|$ denotes the 2-norm and $\Xi_e = \left\{ j \mid \|\mathbf{x}_j - \mathbf{x}_e\| \le r_{\min} \right\}$ refers to the neighborhood set of elements whose centers lie within a circular area specified by the filter radius $r_{\min}$.

2.3 Adjoint equation for linear dynamics

In order to utilize gradient-based optimization algorithms to solve the optimization problem in equation (5), the sensitivities of the objective and constraints with respect to the design variables are needed. These can be obtained efficiently using the standard discrete adjoint method [53]. Before proceeding, we remark that although the objective function in equation (5) is specifically stated, it contains a frequency dependence that reveals some important general features in the context of adjoint analysis. Hence, the conclusions of the presented study are readily extendible to other frequency-dependent objective functions. Following the standard adjoint approach for complex linear systems, the sensitivity of the objective function with respect to design variable ρ_e can be obtained as

$$\frac{\partial J}{\partial \rho_e} = \sum_i^{N_f} \frac{\partial J_i}{\partial \rho_e} \Big/ \left(J_i * \ln(10)\right), \quad \frac{\partial J_i}{\partial \rho_e} = 2\,\mathrm{Re}\left(\boldsymbol{\lambda}(\omega_i)^{\mathrm{T}} \frac{\partial \mathbf{S}(\rho_e, \omega_i)}{\partial \rho_e} \mathbf{U}(\omega_i) \right) \tag{10}$$

where $\boldsymbol{\lambda}(\omega_i)$ is the adjoint vector which satisfies

$$\mathbf{S}(\omega)\boldsymbol{\lambda}(\omega) = -\mathbf{L}\bar{\mathbf{U}}(\omega) \tag{11}$$

where $\bar{\mathbf{U}}(\omega)$ is the complex conjugate of the amplitude vector $\mathbf{U}(\omega)$, where we have utilized that $\mathbf{S}(\omega)$ is a symmetric matrix. From equation (11) it is seen that the adjoint equation differs from the forward problem in the sense that the right-hand-side is frequency dependent. This difference will be shown to have a significant impact on the accuracy of the sensitivities if reusing the basis computed for the state problem for the adjoint problem. This will be discussed in section 4.3.3.

3 Reduced-order methods (ROMs)

In this section, the studied reduced-order methods are briefly presented and discussed, including pseudocodes for each of the ROMs for easy implementation and reproduction of results.

3.1 Projection-based ROMs vs. explicit ROMs

Modal superposition methods [34] have been widely used for the past several decades and show successful applications in many engineering problems. However, the modal superposition methods become less effective in the mid or high-frequency range as the modal density and modal overlap increase. Researchers subsequently developed the modal acceleration method [35] and the hybrid expansion methods [37,54,55] to remedy this shortcoming by employing power series expansion to approximate the high order modes. However, they still have limitations for certain problems, especially for non-proportional damping models. Moreover, solving the global eigenvalue problem is cost-prohibitive for large-scale systems due to the sheer size of the resulting linear systems. Furthermore, eigenvectors that are orthogonal to the loading are not excited even if their frequencies are contained in the loading frequency bandwidth. Hence, many of the expensively computed modes are not even used actively in the reduction. If the considered frequency range is large, large sets of eigenvectors are needed to accurately span the subspace which further reduces the numerical efficiency.

Another computational technique is to compute the solution at a few frequencies (expansion points) and then to determine the behavior at intermediary points by interpolating the response in the neighborhood. Taylor series and Padé expansions [56,57] are two notable venues for constructing interpolants around an expansion point, and the use of Padé approximation versus more classical Taylor series expansions is motivated by the fact that the response function has singular points (poles) where the Taylor series expansion does not converge. However, as reported in Ref. [41], the Padé expansion method leads to an ill-conditioned problem when increasing the expansion order, thus limiting the range of convergence and applicability. A brief description of the Padé expansion method is presented in section 3.4.

In recent years, projection-based reduced-order methods were developed and exploited for fast frequency sweeps. This approach focuses on the construction of a reduced sequence of vectors spanning a subspace on which the FE system can be projected, thus leading to a frequency sweep involving a reduced-size system. The orthonormality of the projection matrix preserves symmetry and definite properties of the system matrices, such that definiteness and stability are preserved for the ROM as well. Assuming the reduced subspace is represented by $\mathbf{Q}_n$, then by pre-multiplying $\mathbf{Q}_n$ into the dynamic equation (2), the state equation can be rewritten as:

$$\left(-\omega^2\mathbf{M}_R + i\omega\mathbf{C}_R + \mathbf{K}_R\right)\mathbf{U}_R(\omega) = \mathbf{F}_R \tag{12}$$

with

$$\mathbf{K}_R=\mathbf{Q}_N^{\mathrm{H}}\mathbf{K}\mathbf{Q}_N,\ \mathbf{C}_R=\mathbf{Q}_N^{\mathrm{H}}\mathbf{C}\mathbf{Q}_N,\ \mathbf{M}_R=\mathbf{Q}_N^{\mathrm{H}}\mathbf{M}\mathbf{Q}_N,\ \mathbf{F}_R=\mathbf{Q}_N^{\mathrm{H}}\mathbf{F} \tag{13}$$

and

$$\mathbf{U}(\omega) = \mathbf{Q}_N^{\mathrm{H}}\mathbf{U}_R(\omega) \tag{14}$$

The dimension of the subspace is *N*, which will be much smaller than the original models' number of degrees of freedom (DOFs). In section 3.2 and section 3.3, four projection-based ROMs, which are proved to have great potential in applications, are listed.

3.2 Quasi-static Ritz vector method (QSRV)

The Ritz vector method was firstly developed by Wilson et al. [58] by constructing its reduction basis vectors using the external force **F**, mass matrix **M**, and stiffness matrix **K**. The sequence of steps to generate the Ritz vector follows as

$$\begin{cases} \mathbf{P}_0 \bar{\mathbf{q}}_0 = \mathbf{F} \\ \mathbf{P}_0 \bar{\mathbf{q}}_j = -\mathbf{P}_2 \mathbf{q}_{j-1} \quad for\ j = 1,...,N-1 \end{cases} \tag{15}$$

with

$$\begin{cases} \mathbf{P}_0 = \mathbf{K} \\ \mathbf{P}_2 = -\mathbf{M} \end{cases} \tag{16}$$

where $\mathbf{q}_j$ is mass-orthogonalized and normalized from $\bar{\mathbf{q}}_j$ at each step, and the reduced space $\mathbf{Q}_N$ can be written as

$$span\{\mathbf{Q}_N\} = span\{\mathbf{q}_0, \mathbf{q}_1, \mathbf{q}_2, ..., \mathbf{q}_{N-1}\}\ . \tag{17}$$

Research [59] showed that this method retains the good convergence characteristics of the modal acceleration method (MCM) but with a much smaller computational cost. However, the Ritz vector method is only suited for relatively low-frequency problems. For solving high-frequency problems or wide-band problems, a tuning parameter, designated as the expansion frequency, is introduced in the quasi-static Ritz vector (QSRV) method [42,60] which incorporates inertial effects in the first order problem. This renders the method suitable for arbitrary frequency ranges of interest. The formulation (16) is modified to

$$\begin{cases} \mathbf{P}_0 = -\omega_0^2 \mathbf{M} + \mathbf{K} \\ \mathbf{P}_2 = -\mathbf{M} \end{cases} \tag{18}$$

where ω_0 is the expansion frequency located in the frequency range of interest. Usually, it is chosen at the midpoint of the frequency range. This procedure is also named the shifted Ritz vector method. In this procedure, the damping matrix is ignored. As a matter of convenience, this procedure is abbreviated as **QSRV** for the remainder of this manuscript.

In Ref. [61] a modified QSRV procedure was proposed to include damping effects, such that equation (18) is modified to

$$\begin{cases} \mathbf{P}_0 = -\omega_0^2 \mathbf{M} + i\omega_0 \mathbf{C} + \mathbf{K} \\ \mathbf{P}_2 = -\mathbf{M} \end{cases}\ . \tag{19}$$

In the following, this procedure is named **QSRV_D.**

Note that, in the recurrence procedure, the matrix $\mathbf{P}_0$ remains unchanged and can be decomposed in advance. Thus, generating *N* basis vectors is very fast and much less expensive than normal modes. The pseudocodes of the **QSRV** and the **QSRV_D** are identical and are found stated in Algorithm 1. The only difference is the definition of $\mathbf{P}_0$ as given in equation (18) or equation (19) for the QSRV and QSRV_D, respectively.

Algorithm 1 [Quasi-static Ritz vector method (**QSRV** and **QSRV_D**)]

1. Solve $\mathbf{P}_0\bar{\mathbf{q}}_0=\mathbf{F}$
2. $\mathbf{q}_0=\bar{\mathbf{q}}_0\Big/\sqrt{\bar{\mathbf{q}}_0^{\mathrm{H}}\mathbf{M}\bar{\mathbf{q}}_0}$
3. for j = 1, 2, …, N-1, do
4. solve $\mathbf{P}_0\bar{\mathbf{q}}_j=-\mathbf{P}_2\mathbf{q}_{j-1}$
5. $\mathbf{p}=\bar{\mathbf{q}}_j$
6. for i = 0,1, …, j-1, do
7. $\bar{\mathbf{q}}_j=\bar{\mathbf{q}}_j-\left(\mathbf{p}^{\mathrm{H}}\mathbf{M}\mathbf{q}_i\right)\mathbf{q}_i$
8. end for
9. $\mathbf{q}_j=\bar{\mathbf{q}}_j\Big/\sqrt{\bar{\mathbf{q}}_j^{\mathrm{H}}\mathbf{M}\bar{\mathbf{q}}_j}$
10. end for
11. Output $\mathbf{Q}_N=span\{\mathbf{q}_0,\mathbf{q}_1,\mathbf{q}_2,...,\mathbf{q}_{N-1}\}$

The for-loop in lines 6–8 constitute the mass-orthogonalization procedure with respect to the $\{\mathbf{q}_i\}$ vectors.

3.3 Second-order Krylov subspace method

The Krylov subspace method [43,44] was initially developed for the iterative solution of large-scale sparse linear systems and linear eigenvalue problems. It is generated by a sequence of vectors defined via a first-order linear homogeneous recurrence relation and demonstrates superiority in generating an orthonormal basis with excellent convergence behavior. Nevertheless, the considered problem equation (2) is a second-order system. Thus, in order to apply the Krylov method directly, it should first be rewritten as a first-order system, i.e.

$$\left(\begin{bmatrix}\mathbf{C} & \mathbf{K}\\ -\mathbf{I} & \mathbf{0}\end{bmatrix}+i\omega\begin{bmatrix}\mathbf{M} & \mathbf{0}\\ \mathbf{0} & \mathbf{I}\end{bmatrix}\right)\begin{bmatrix}i\omega\mathbf{U}\\ \mathbf{U}\end{bmatrix}=\begin{bmatrix}\mathbf{F}\\ \mathbf{0}\end{bmatrix}. \tag{20}$$

where $\mathbf{0}$ and $\mathbf{I}$ represent the zero and the identity matrices, respectively. Using this form, the Krylov subspace method can be applied directly. However, following this path doubles the size of the linear systems involved in the formulation of the original frequency sweep problem and may also destroy some of its characteristics, such as symmetry and positive definiteness. For solving this issue, the second-order Krylov subspace method can be employed to avoid solving Eq. (20). It spans the subspace at the expansion frequency ω_0 by:

$$\begin{cases}\mathbf{P}_0\bar{\mathbf{q}}_0=\mathbf{F}\\ \mathbf{P}_0\bar{\mathbf{q}}_1=-\mathbf{P}_1\mathbf{q}_0\\ \mathbf{P}_0\bar{\mathbf{q}}_j=-\mathbf{P}_1\mathbf{q}_{j-1}-\mathbf{P}_2\mathbf{q}_{j-2}\quad for\ j=2,...,N-1\end{cases} \tag{21}$$

with

$$\begin{cases}\mathbf{P}_0=\mathbf{S}(\omega_0)=-\omega_0^2\mathbf{M}+i\omega_0\mathbf{C}+\mathbf{K}\\ \mathbf{P}_1=\dfrac{\partial\mathbf{S}}{\partial\omega}(\omega_0)=i\mathbf{C}-2\omega_0\mathbf{M}\\ \mathbf{P}_2=\dfrac{1}{2}\dfrac{\partial^2\mathbf{S}}{\partial\omega^2}(\omega_0)=-\mathbf{M}\end{cases} \tag{22}$$

where $\mathbf{q}_j$ is orthogonalized and normalized from $\bar{\mathbf{q}}_j$ at each step. Previous studies have shown that the generated set of basis vectors will lose their internal orthogonality due to numerical rounding errors as the size of the subspace is increased. This in turn leads to an ill-conditioned reduction matrix which lacks robustness and can result in convergence stagnation. Therefore, it is very important to choose the orthonormalization method properly. To investigate this phenomenon, three different widely used strategies to construct the orthonormal basis vectors of $\mathbf{Q}_N = span\{\mathbf{q}_0, \mathbf{q}_1, \mathbf{q}_2, ..., \mathbf{q}_{N-1}\}$ are presented and compared by numerical experiments. In the following subsections, 3.3.1 to 3.3.3, the three orthonormalization algorithms are described for the second-order Krylov subspace method.

3.3.1 Modified Gram-Schmidt orthonormalization

The simplest orthogonalization procedure is to directly apply the modified Gram–Schmidt on the reduced basis vectors obtained in equation (21). In order to distinguish the three different second order Krylov methods, we choose to abbreviate the approaches based on their normalization procedure. Hence, the Second Order Krylov method with Modified Gramm-Schmidt is named **SOMG** and the procedure can be written in pseudocode as:

Algorithm 2 [Second-order Krylov subspace method with modified Gram-Schmidt orthonormalization (**SOMG**)]

1. Solve $\mathbf{P}_0 \bar{\mathbf{q}}_0 = \mathbf{F}$
2. $\mathbf{q}_0 = \bar{\mathbf{q}}_0 / \|\bar{\mathbf{q}}\|_2$
3. for j = 1, 2, …, N-1, do
4. if j=1
5. solve $\mathbf{P}_0 \bar{\mathbf{q}}_j = -\mathbf{P}_1 \mathbf{q}_{j-1}$
6. else
7. solve $\mathbf{P}_0 \bar{\mathbf{q}}_j = -\mathbf{P}_1 \mathbf{q}_{j-1} - \mathbf{P}_2 \mathbf{q}_{j-2}$
8. end if
9. for i = 0,1, …, j-1, do
10. $\bar{\mathbf{q}}_j = \bar{\mathbf{q}}_j - \langle \bar{\mathbf{q}}_j, \mathbf{q}_i \rangle \mathbf{q}_i$
11. end for
12. $\mathbf{q}_j = \bar{\mathbf{q}}_j / \|\bar{\mathbf{q}}_j\|_2$
13. end for
14. Output $\mathbf{Q}_N = span\{\mathbf{q}_0, \mathbf{q}_1, \mathbf{q}_2, ..., \mathbf{q}_{N-1}\}$

The lines 1-2 and 4-8 constitute the second-order Krylov procedure and the for-loop in lines 9–11 is the Gramm-Schmidt orthogonalization procedure with respect to the $\{\mathbf{q}_i\}$ vectors. $\langle \bullet, \bullet \rangle$ represents the inner product of two vectors, $\|\bullet\|_2$ denotes the 2-norm of a vector.

3.3.2 Moment-matching Gram-Schmidt orthonormalization

Slone et al. [62] found that the modified Gram-Schmidt orthonormalization will destroy the moment matching, which causes failure for certain problems or narrows the bandwidth of accuracy for the resulting reduced order system. This is also verified in the second example (section 4.3) of this study. To remedy this issue, a moment-matching method [63] was developed, which orthonormalized the basis vectors generated at each step using a correction term for the right-hand side of the recurrence procedure in equation (21). We abbreviate this procedure as **SOMMG**, and the pseudocode follows as:

Algorithm 3 [Second-order Krylov subspace method with moment-matching Gram-Schmidt orthonormalization (**SOMMG**)]

1. Solve $\mathbf{P}_0\bar{\mathbf{q}}_0 = \mathbf{F}$
2. $\mathbf{U}_{[0,0]} = \|\bar{\mathbf{q}}\|_2$, $\mathbf{q}_0 = \bar{\mathbf{q}}_0 / \mathbf{U}_{[0,0]}$
3. for j = 1, 2, …, N-1, do
4. if j=1
5. solve $\mathbf{P}_0\bar{\mathbf{q}}_j = -\mathbf{P}_1\mathbf{q}_{j-1}$
6. else
7. solve $\mathbf{P}_0\bar{\mathbf{q}}_j = -\mathbf{P}_1\mathbf{q}_{j-1} - \mathbf{P}_2\mathbf{Q}_{j-2}\mathbf{U}^{-1}_{[1:j-1,1:j-1]}\mathbf{e}_{j-1}$
8. end if
9. for i = 0,1, …, j-1, do
10. $\mathbf{U}_{[i,j]} = \langle\bar{\mathbf{q}}_j, \mathbf{q}_i\rangle$, $\bar{\mathbf{q}}_j = \bar{\mathbf{q}}_j - \mathbf{U}_{[i,j]}\mathbf{q}_i$
11. end for
12. $\mathbf{U}_{[j,j]} = \|\bar{\mathbf{q}}_j\|_2$, $\mathbf{q}_j = \bar{\mathbf{q}}_j / \mathbf{U}_{[j,j]}$
13. end for
14. Output $\mathbf{Q}_N = span\{\mathbf{q}_0, \mathbf{q}_1, \mathbf{q}_2, ..., \mathbf{q}_{N-1}\}$

Consistent with Algorithm 2, lines 1-2 and 4-8 correspond to the modified second-order Krylov procedure, and the for-loop in lines 9–11 refers to the orthogonalization procedure with respect to the $\{\mathbf{q}_i\}$ vectors. $\mathbf{U}$ is a $N\times N$ upper triangular, nonsingular matrix containing the modified Gram-Schmidt coefficients. The biggest difference between SOMG and SOMMG is the second term on the right hand in line 7. This term is introduced to ensure moment-matching. Here $\mathbf{e}_{j-1}$ is the unit vector with j-1 entries and the last term is one, and $\mathbf{Q}_{j-2}$ is a matrix spanned by $\{\mathbf{q}_0, \mathbf{q}_1, \mathbf{q}_2, ..., \mathbf{q}_{j-2}\}$.

3.3.3 The Second-Order Arnoldi method

Another possibility is to use an Arnoldi-like procedure for generating the orthonormal basis for the second-order Krylov method. Such an approach is proposed by Bai et al. [64,65] and is named the Second-Order ARnoldi method (**SOAR**) and has the following pseudocode:

Algorithm 4 [Second-Order Arnoldi method (**SOAR**)]

1. Solve $\mathbf{P}_0\mathbf{q}_0 = \mathbf{F}$
2. $\mathbf{q}_0 = \mathbf{q}_0 / \|\mathbf{q}_0\|_2$
3. $\mathbf{p}_0 = \mathbf{0}$
4. for j = 0, 1, …, N-2, do
5. solve $\mathbf{P}_0\mathbf{r} = -\mathbf{P}_1\mathbf{q}_j - \mathbf{P}_2\mathbf{p}_j$
6. $\mathbf{s} = \mathbf{q}_j$
7. for i = 0,1, …, j, do
8. $\mathbf{r} = \mathbf{r} - \langle\mathbf{q}_i, \mathbf{r}\rangle\mathbf{q}_i$
9. $\mathbf{s} = \mathbf{s} - \langle\mathbf{q}_i, \mathbf{r}\rangle\mathbf{p}_i$
10. end for
11. $\mathbf{q}_{j+1} = \mathbf{r} / \|\mathbf{r}\|_2$
12. $\mathbf{p}_{j+1} = \mathbf{s} / \|\mathbf{r}\|_2$
13. end for
14. Output $\mathbf{Q}_N = span\{\mathbf{q}_0, \mathbf{q}_1, \mathbf{q}_2, ..., \mathbf{q}_{N-1}\}$

Here, lines 1-3 and 5-6 correspond to the second-order Krylov procedure, and the for-loop in lines 7–10 is the orthogonalization procedure with respect to the $\{\mathbf{q}_i\}$ vectors. The additional vector sequence $\{\mathbf{p}_i\}$ is an auxiliary sequence and is intended to have the same effect on the Krylov expansion as the correction term used for the SOMMG procedure.

3.3.4 Other orthogonalization algorithms

Apart from the above three orthogonalization algorithms, some other methods, i.e., Singular Value Decomposition (SVD) method [66], can also be employed. However, due to numerical rounding errors, the problems often become ill-conditioned using SVD. We can get accurate solutions only in a narrow frequency range, even though a large number of basis vectors are used. Furthermore, for constructing a proper ROM, it is essential to orthogonalize the basis vectors in each step, applied to generate the next basis vectors.

3.4 Padé approximant method

For completeness, a brief description of the Padé approximant method is given in this section. As given in Ref. [41], the solution of a vibration problem with harmonic excitation can be expressed in the Padé approximants as

$$\mathbf{U}(\omega)=\frac{\mathbf{r}_0+\sum_{i=1}^{N-1}\mathbf{a}_i(\omega-\omega_0)^i}{1+\sum_{i=1}^{N-1}b_i(\omega-\omega_0)^i} \tag{23}$$

where $\mathbf{r}_0$, $\mathbf{a}_i$ and b_i are the unknown parameters. Substituting equation (23) into equation (2) and the terms are matched by order of $(\omega-\omega_0)$. The following set of equations can be obtained:

$$\begin{cases}\mathbf{P}_0\mathbf{r}_0=\mathbf{F}\\ \mathbf{P}_0\mathbf{r}_1=-\mathbf{P}_1\mathbf{r}_0\\ \mathbf{P}_0\mathbf{r}_l=-\mathbf{P}_1\mathbf{r}_{l-1}-\mathbf{P}_2\mathbf{r}_{l-2}, \quad for\ l\geq 2\end{cases} \tag{24}$$

where $\mathbf{P}_0$, $\mathbf{P}_1$ and $\mathbf{P}_2$ are consistent with the formulation (22) and the parameters $b_1, b_2, \ldots, b_{N-1}$ are obtained by pseudoinverse

$$[\mathbf{r}_{n-1},\mathbf{r}_{n-2},....,\mathbf{r}_1]\begin{pmatrix}b_1\\ b_2\\ \\ b_{N-1}\end{pmatrix}=-\mathbf{r}_N \tag{25}$$

Subsequently, the parameter vectors $\mathbf{a}_1,\mathbf{a}_2,.....,\mathbf{a}_{N-1}$ are computed by

$$\begin{aligned}\mathbf{a}_1&=\mathbf{r}_1+b_1\mathbf{r}_0\\ \mathbf{a}_i&=\mathbf{r}_i+\sum_{j=1}^{i-1}b_j\mathbf{r}_{i-j}+b_i\mathbf{r}_1, \quad i=2,....,N-1\end{aligned} \tag{26}$$

After the parameters $\mathbf{r}_0$, $\mathbf{a}_i$ and b_i are obtained, the explicit formulation of $\mathbf{U}(\omega)$ can be written according to equation (23).

4 Numerical examples

To investigate the performance of the different ROMs in the context of topology optimization, the methods are first evaluated based on their ability to solve the state and the adjoint problems for a wide frequency range. Thereafter the methods are used to solve two model optimization problems, i.e. a vibration suppression problem and a wave propagation problem, and the results are compared based on both objective function values and the layout of the optimized designs as well as CPU time savings. In all numerical test cases, the ROM solutions are compared to the full model solution. However, in order to estimate and compare the performance of different ROMs for solving the harmonic problems, an error-index estimation measure is first introduced.

4.1 Error estimation

To evaluate and plot the solutions as function of frequency, the vector 2-norm is applied to the displacement and adjoint vectors, i.e.

$$A(\omega) = \left\|\mathbf{U}(\omega)\right\|_2 \quad \text{or} \quad \left\|\boldsymbol{\lambda}(\omega)\right\|_2 \tag{27}$$

To assess the accuracy of the ROMs with respect to the reference (full) solution, a relative error indicator is introduced in this work as:

$$\varepsilon(\omega) = \frac{\left\|\mathbf{U}_{ROM}(\omega) - \mathbf{U}_{Full}(\omega)\right\|_2}{\left\|\mathbf{U}_{full}(\omega)\right\|_2} \quad \text{or} \quad \frac{\left\|\boldsymbol{\lambda}_{ROM}(\omega) - \boldsymbol{\lambda}_{Full}(\omega)\right\|_2}{\left\|\boldsymbol{\lambda}_{full}(\omega)\right\|_2} \tag{28}$$

where subscripts *ROM* and *Full* denote the solutions yield by the ROMs and the full models, respectively.

The width of the frequency range of valid approximation is related to the number of basis vectors. We define this frequency range $\left[\omega_{\inf}, \omega_{\sup}\right]$ of the approximation by the ROM method at order *N* as the interval where:

$$\varepsilon(\omega) \le \varepsilon_{\max} \tag{29}$$

where $\varepsilon_{\max}$ is a small threshold value with $\varepsilon_{\max} = 0.01$ used in this work. Here 0.01 is chosen according to the solutions in the following numerical examples. When solving the state equation, for a prescribed order *N*, there is a quite distinct boundary between the frequency range that can be or cannot be well approximated. Thus, the frequency range $\left[\omega_{\inf}, \omega_{\sup}\right]$ obtained by 0.01 or a much smaller value, for example 0.0001, is nearly the same. However, the relative errors of the solutions for the adjoint equation are much larger than the solution of the state equation. If we choose a too small threshold value, the frequency range $\left[\omega_{\inf}, \omega_{\sup}\right]$ will be restrictively narrow. As is shown in Fig. 26 b) and Fig. 27 b), in most of the range, the $\varepsilon(\omega)$ of SOMMG and SOAR are just slighly below 0.01, but this turns out to be enough to obtain a satisfactory topology optimization result, as shown in Table 7 and Table 8. Based on the above discussion, we think $\varepsilon_{\max} = 0.01$ is appropriate and is suggested to be used to evaluate a ROM.

4.2 Example 1: vibration problem

The first numerical example concerns the vibration of a sandwich beam shown in Fig. 1. The size of the beam is 1.2m ×0.3m and the beam is doubly clamped, meaning that the left and right sides are fully fixed. A harmonic excitation is introduced by a force **F**=1e9N applied in the middle

of the upper side as shown in the figure. The frequency band of interest is from 0 to 30000 rad/s which for the reference solution is divided into discrete frequencies using an interval of 30 rad/s. The model problem used to study the state and adjoint solutions is based on the two-material layout as shown in Fig. 1. The truss like structure, shown as black consists of material 1 and has a beam width of 0.08m, whereas the cyan part is material 2. The properties of the two materials are listed in Table 1 and the domain is discretized by 240 ×30 bilinear Lagrange elements resulting in 14942 degrees of freedom for the full model. The objective function and adjoint equation are evaluated at the dashed red line. Unless otherwise stated, the expansion frequency point used for the ROMs is the mid-point of the frequency range, i.e. for this example $\omega_0 = 15000$ rad/s. Damping is introduced through the Rayleigh damping model, in which the element damping matrix $\mathbf{C}_e$ takes the form:

$$\mathbf{C}_e = \alpha_e \mathbf{M}_e + \beta_e \mathbf{K}_e \tag{30}$$

where $\mathbf{M}_e$ and $\mathbf{K}_e$ denote the element mass and stiffness matrices, respectively. The damping parameter α_e and β_e refers to the mass-proportional and stiffness-proportional damping constants, respectively, and are likewise stated in Table 1.

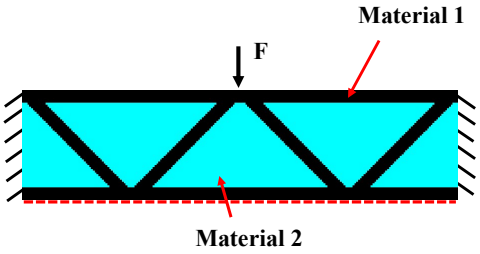

Fig. 1 The sandwich structure in example 1.

Table 1 The material properties in example 1.

Material	Density (kg/m^3)	Modulus (GPa)	Poisson ratio	α_e	β_e
Material 1	11600	40.8	0.37	1e-6	1e-7
Material 2	1180	14.9	0.37	1e-5	1e-6

4.2.1 Solving the state equation

In this subsection, the solution to the state equation for the model problem in Fig. 1 is investigated. The frequency responses using the full model as well as all the different ROMs with 20 basis vectors are shown in Fig. 2. Specifically, in Fig. 2a, the results obtained by the QSRV are shown, whereas Fig. 2b shows the results obtained by the three second-order Krylov based methods (SOMG, SOMMG, and SOAR). The results show that all methods yield accurate approximations in a frequency range close to the expansion frequency point ($\omega_0 = 15000$ rad/s). Furthermore, it is observed that the frequency responses for SOMG, SOMMG, and SOAR are coincident. The results obtained by the QSRV_D and the Padé expansion methods are plotted in Fig. 2a. Results show that the Padé expansion can yield an accurate solution only for a very narrow frequency range, whereas the QSRV_D covers a broader frequency range. However, the result obtained by the QSRV_D is seen to oscillate noticeably for frequencies far away from the expansion point, a shortcoming due to the ill-conditioning of the orthonormal basis vectors.

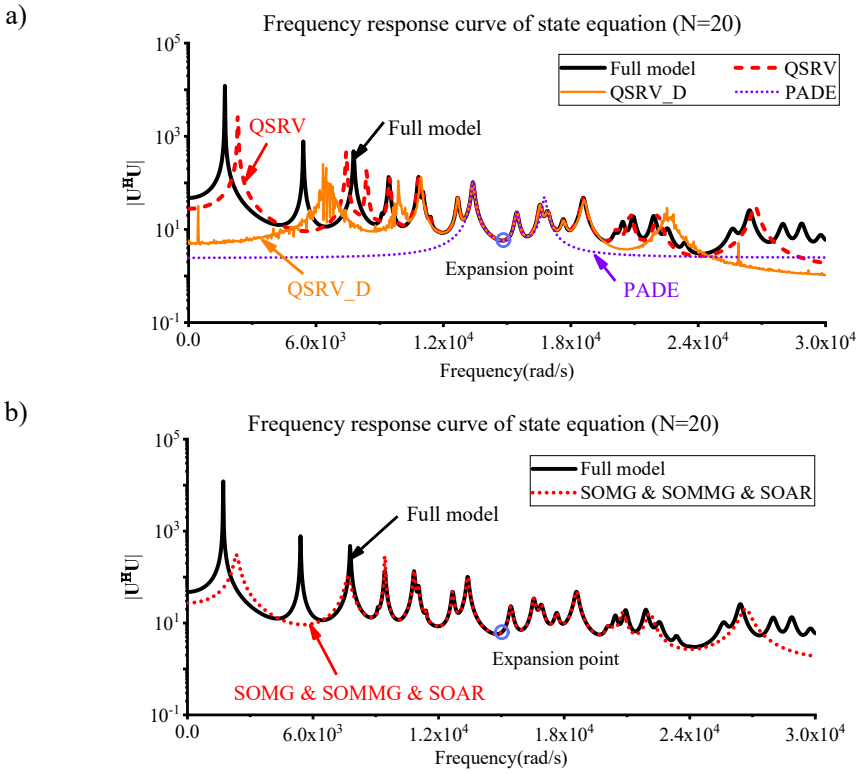

Fig. 2 The frequency responses of the state equation (*N*=20, vibration problem): a) QSRV, QSRV_D and Padé; b) SOMG, SOMMG and SOAR.

Evaluating the results using the relative error measure from equation (24) yields the plots shown in Fig. 3 and the frequency intervals satisfying $\varepsilon < 0.01$ are listed in Table 2 for all the ROMs. From this it is clear that the three second-order Krylov based methods (SOMG, SOMMG, and SOAR) can provide an accurate solution for a larger frequency range than the other methods, and that the Padé approximants only allows for a very narrow frequency range. Furthermore, it is interesting to see the relative errors for the SOMMG and the SOAR are much smaller than for the SOMG, even though the same frequency range obeying $\varepsilon < 0.01$ can be obtained. This clearly shows that the quality of the orthonormalization process has an important influence on precision.

To test the stability and robustness of the different ROMs, the number of the basis vectors is increased from 10 to 70 using an incremental step of 5. The convergence curves are presented in Fig. 4, where the *x*-axis refers to the number of the basis vectors *N,* and the *y*-axis refers to the frequency range satisfying $\varepsilon(\omega) \le 0.01$. For the first four methods (QSRV, SOMG, SOMMG, and SOAR), it is seen that the frequency range covered can be increased by increasing the number of basis vectors. In fact, using 50 basis vectors means that the whole frequency range of interest (0-30000 rad/s) can be approximated within the desired tolerance. However, this is not true for the QSRV_D and the Padé approximants, for which only a narrow frequency band can be approximated. Also, it is seen that increasing the number of the basis vector does not improve significantly on the width of the frequency range. The primary cause is that the high order basis vectors lose orthogonality due to numerical rounding errors, meaning that these additional vectors no longer contribute to the solution. Due to these results, the reader should note that the QSRV_D and Padé are not tested anymore in the following sections.

Table 2 The frequency intervals satisfy $\varepsilon < 0.01$ for different ROMs with *N*=20

Methods / Frequency (rad/s)	QSRV	SOMG	SOMMG	SOAR	QSRV_D	PADE
Lower limit	11460	11250	11250	11250	12200	14430
Upper limit	18360	19530	19530	19530	17100	15300
Range	6900	8280	8280	8280	4900	870

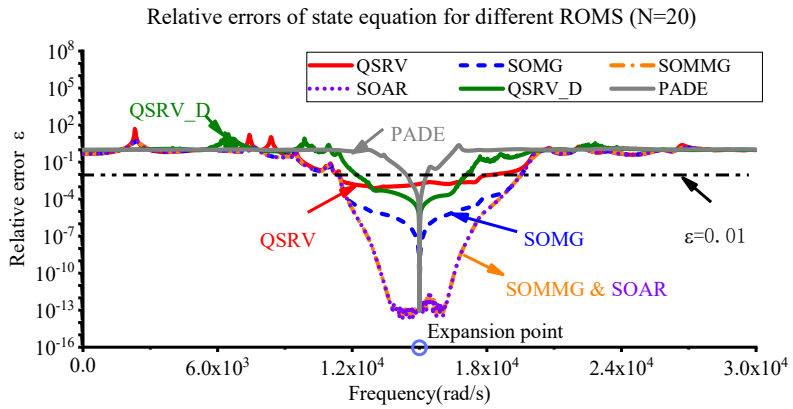

Fig. 3 Relative errors of solving the state equation for different ROMs (*N*=20, vibration problem).

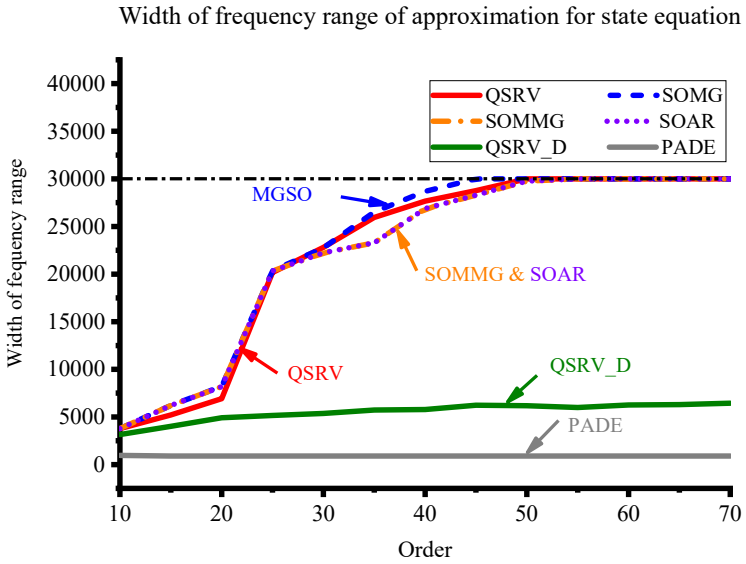

Fig. 4 Width of the frequency range as a function of the number of basis vectors for different ROMs when solving the state equation (vibration problem).

4.2.2 Solving the adjoint equation

In this subsection, the ROMs are used to solve the adjoint equation which is essential for all non-self-adjoint topology optimization problems. Although the adjoint equation has the same system matrix as the state problem, the adjoint problem differs due to a frequency-dependent (amplitude-dependent) force vector. To investigate the consequence of this difference, the frequency responses of the adjoint equation for different ROMs with *N*=40 are shown in Fig. 5. From these graphs, it is found that the second-order Krylov based methods (SOMG, SOMMG, and SOAR) perform much better than the QSRV. That is, the responses obtained by all three second-order Krylov

based methods nearly coincide with the full model, whereas the QSRV only covers around one-third of the frequency range centered at expansion frequency.

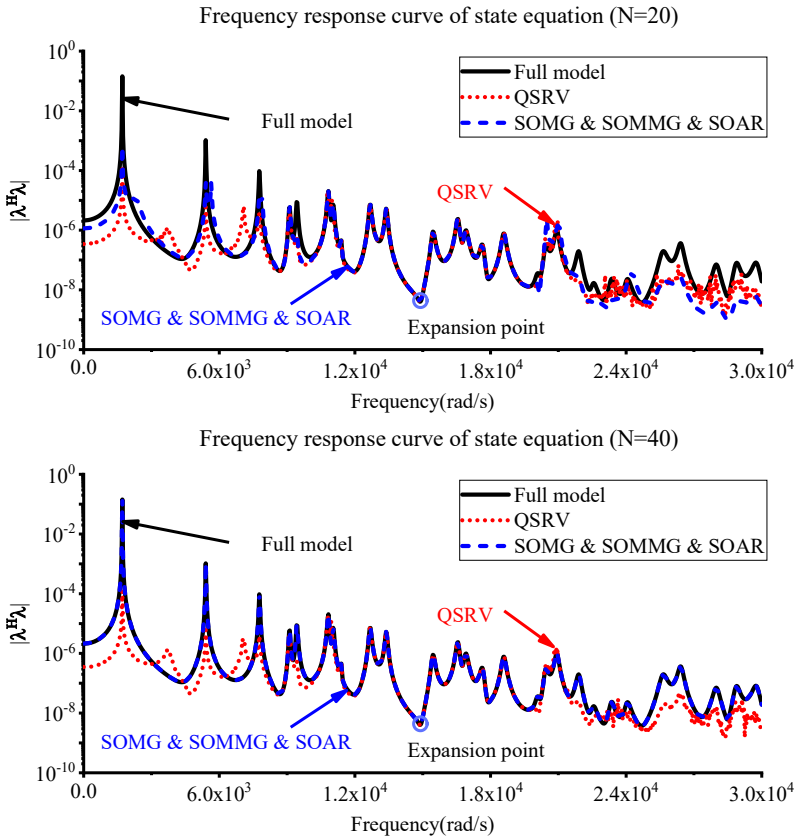

Fig. 5 The frequency response of the adjoint equation for different ROMs (*N*=20 and 40, vibration problem).

Fig. 6 presents the relative errors of the ROMs based on the error measure from equation (24). The results show that the relative errors of the results obtained by the QSRV method are very large for most of the frequency range. Even in the vicinity of the expansion point, the errors are significantly larger than $\varepsilon = 0.01$. For the other three ROMs, the majority of relative errors are smaller than 0.01, especially for the low frequency range. Moreover, for most of the frequency range, the error remains smaller than 0.1.

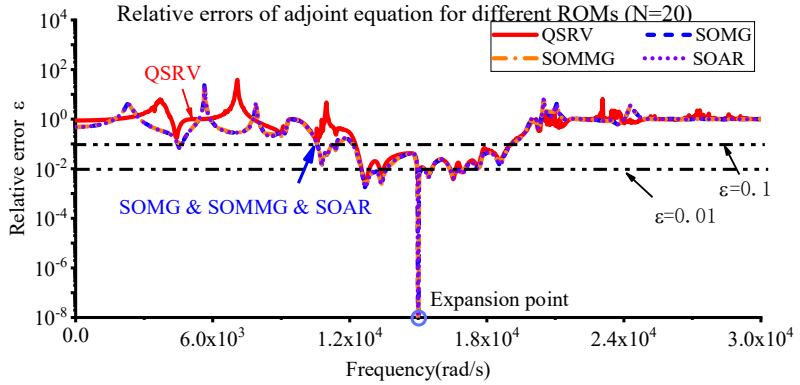

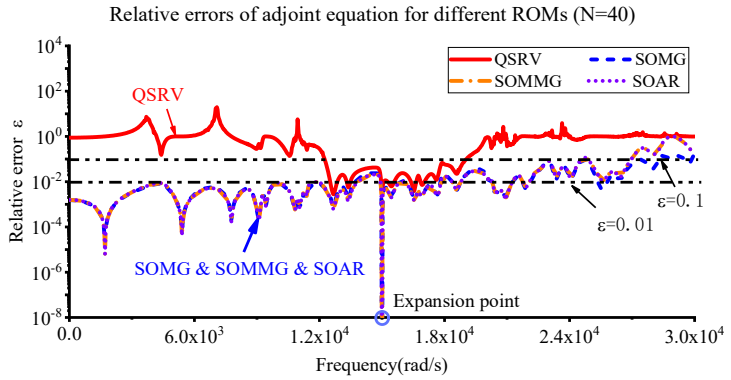

Fig. 6 Relative errors for solving the adjoint equation (*N*=20 and 40, vibration problem).

The width of the frequency range as a function of the number of basis vectors is presented in Fig. 7 for the four ROMs. From these graphs, we find that the QSRV algorithm fails in covering the desired frequency range to a satisfactory tolerance. This means, for topology optimization, that the QSRV can yield a sufficiently accurate solution of the state equation by increasing the number of basis vectors, but that it will fail to solve the adjoint equation over a broad frequency band. For the SOMG, SOMMG, and SOAR models it is seen that by increasing the size of the spanned subspace, the reduced-order model can enlarge the range of acceptable approximate solutions. Moreover, the SOMMG and SOAR show better properties than SOMG. However, it is also seen that none of the methods are able to cover the entire spectrum of interest using only a single expansion point. This is because the force vector is frequency dependent and hence that the solution for the expansion point is a poor representation of especially the high frequency adjoint response. To solve this issue, a multi expansion points strategy can be used, however, this is deemed outside of the scope of this article.

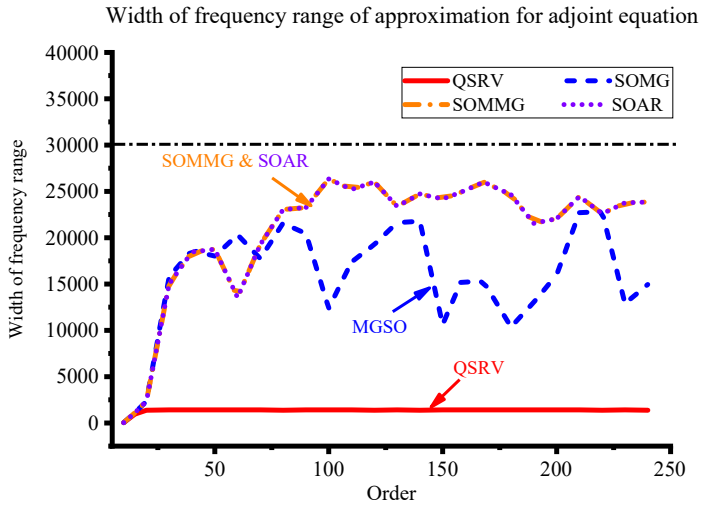

Fig. 7 Width of the frequency range as a function of the number of basis vectors for different ROMs when solving the adjoint equation (vibration problem).

4.2.3 Computational cost

In this subsection, discussions about the computational cost of different ROMs are presented using a 3D problem shown in Fig. 8. The material properties and the sizes in the x and y directions are the same as the example discussed before. The used element size is 0.01, and the frequency band of interest is from 0 to 20000 rad/s, divided into discrete frequencies using an interval of 50 rad/s.

The number of elements is 18 000 and the number of dofs is 67 518. The expansion frequency point used for the ROMs is the mid-point of the frequency range ω_0 =20000 rad/s. Firstly, the thickness *Lz*=0.05 is applied, and numerical solutions show that 35 basis vectors in the ROMs ensure the approximate solutions. The frequency response curve solved by the full model and the relative errors of the four ROMs (*N*=35) are shown in Fig. 9 a) and b), respectively. The results coincide with the conclusions in the 2D problems.

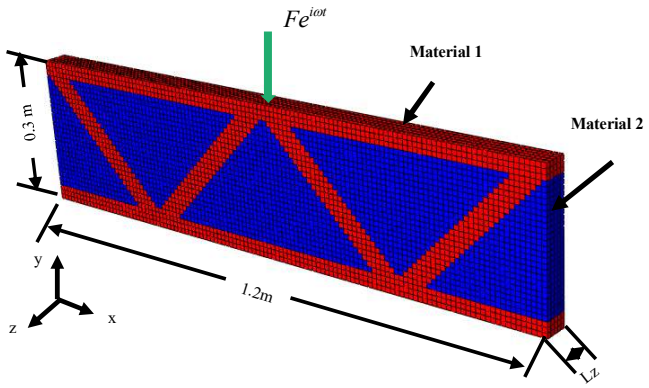

Fig. 8 The 3D sandwich structure for testing the computational cost

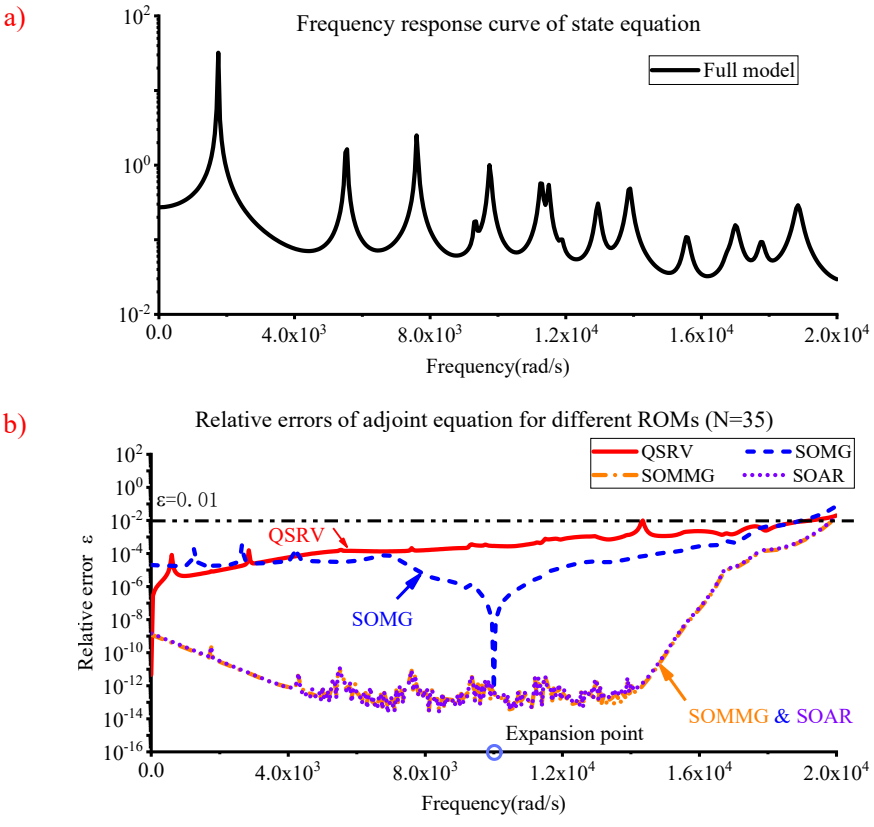

Fig. 9 The frequency response curve solved by the full model and the relative errors of the four ROMs

The time-cost of a ROM can be divided into two parts. The first part is constructing the basis vectors, and the second part is the frequency sweep of the reduced model. These are represented by

T_{bv} and T_{fs}, respectively. The time cost of the frequency sweep T_{fs} is linearly related to the number of frequency points in the considered frequency range. To test the influence of the finite element resolution, the model is progressively refined by increasing the size in the *z*-direction *Lz*. Here, the cases *Lz* = 0.05, 0.10, 0.15, 0.20, 0.25 are studied, which corresponds to 67 518, 123 783, 180 048, 236 313, and 292 578 dofs, respectively. Numerical examples show that the conclusion for 2D in sections 4.2.1 and 4.2.2 are also valid for the increased resolution, and due to space limitations, these will not be shown. Furthermore, unless specific stated, the following results are obtained for solving the state equation. However, the conclusions hold also for solving the adjoint equation.

Fig. 10 presents the time-costs of the different ROMs for different resolutions in constructing the basis vectors and frequency sweep. Here 401 frequency points are applied to discretize the frequency range. Fig. 11 a) shows that, in constructing the basis vectors, SOMG, SOMMG, and SOAR are more time costly than QSRV. This is due to the complex number equations to be solved, yet only real number equations are solved in QSRV. For the frequency sweep, from Fig. 11 b), we find an increased cost of QSRV, mainly since the linear equation of the reduced model obtained by QSRV becomes nearly singular, which increases the time-cost in solving the linear equation. From Fig. 10 we can find that most of the time is spent on constructing basis vectors using the ROMs to solve the large-scale problem. Thus efficient techniques to solve large-scale linear equations mentioned in the introduction should be applied in further studies.

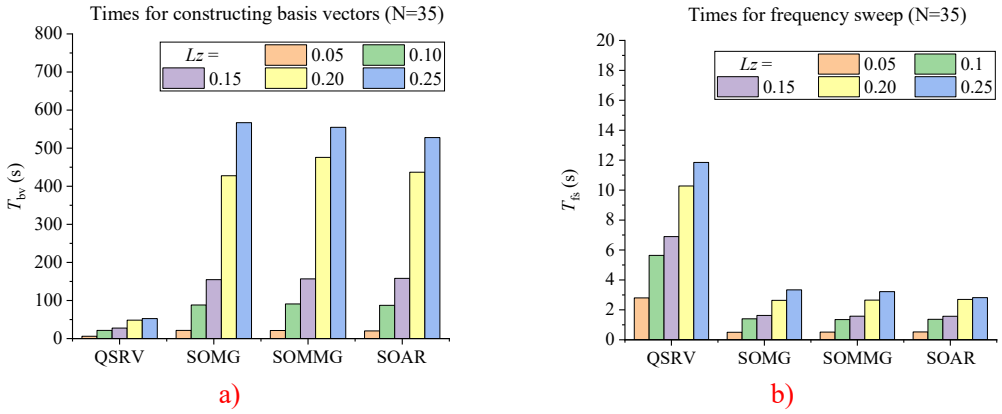

Fig. 10 The time costs of different ROMs in constructing the basis vectors and frequency sweep. 401 frequency points are used to discretize the frequency range (*Lx*=1.2, *Ly*=0.3, and the element size are 0.05).

a) Times for constructing basis vectors, b) Times for frequency sweep.

Next, we discuss how much computational cost can be saved by using the ROMs. In this study, we take the SOAR method as an example. T_{FULL} and T_{SOAR} represent the computational time of the full model and SOAR, respectively. Fig. 11 shows the curves of T_{SOAR}/T_{FULL} with the variation of the number of frequency points in the considered frequency range for different resolutions. It can be found that when the number of frequency points is small, the time-cost of the SOAR will approach the full model due to the time cost in constructing the basis vectors. However, with increase of the number of frequency points, the time ratio drops quickly. For the fine resolution, for example, *Lz*=0.25 (292 578 dofs) with 4000 frequency points, the computational cost is only 0.05 % of the full model.

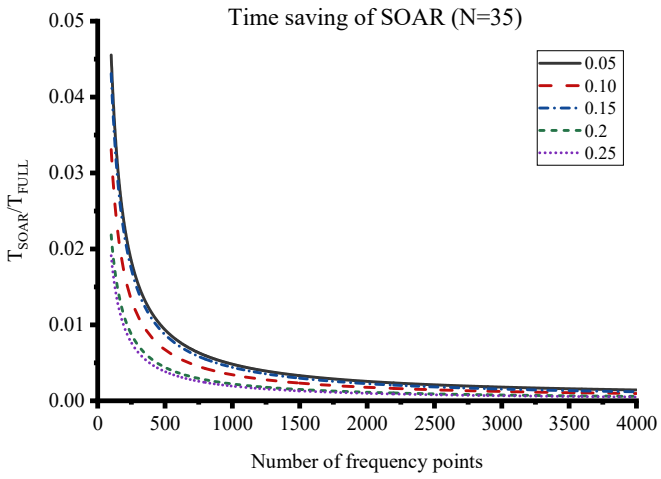

Fig. 11 The curves of T_{SOAR}/T_{FULL} with the variation of the frequency points in the considered frequency range for different resolutions.

4.2.4 Topology optimization results

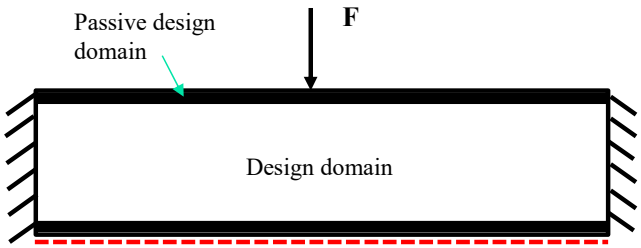

Fig. 12 Illustration of the design domain (vibration suppression problem) for which the objective function is evaluated at the dashed red line.

In this section, the optimized designs and their objective values for the vibration suppression problem are investigated for the different ROMs and compared to the full solution. The optimization problem is based on the model problem from Fig. 2 and is shown in Fig. 12 where the objective function is evaluated at the dashed red line. Furthermore, the upper and bottom three layers of elements are set as passive design domains using material 1, and all other material parameters are as listed in Table 1. A harmonic excitation is introduced by a force **F**=1e14N applied in the middle of the upper side as shown in the figure. To regularize the design problem, a Heaviside density filter is applied using a filter radius of 5.5 times the element size. The projection parameter η in the smooth Heaviside function is chosen as 0.5, and the steepness parameter β is updated as $\beta = 2\beta$ from an initial value of 1 at every 50 steps up to 128. Two cases covering different frequency bands are considered in this study, and the optimized designs are listed in Table 3 and Table 4, respectively. The optimized designs obtained by the full model as defined as the reference solutions. The numbers under the results are the objective function values given by equation (5), where the first number is the objective value computed by the full model, and the number in parentheses corresponds to that predicted by the ROM.

In case 1, the considered frequency interval is $\omega \in$ [0, 1e4] rad/s, and it is discretized by 201 frequency points. Case 2 is a high-frequency problem, in which the considered frequency interval is $\omega \in$ [0, 3e4] rad/s with 401 frequency points. The frequency responses of the optimized designs

obtained by the full model are presented in Fig. 13. Nearly 4 four peaks exist in case 1, and many more peaks in case 2.

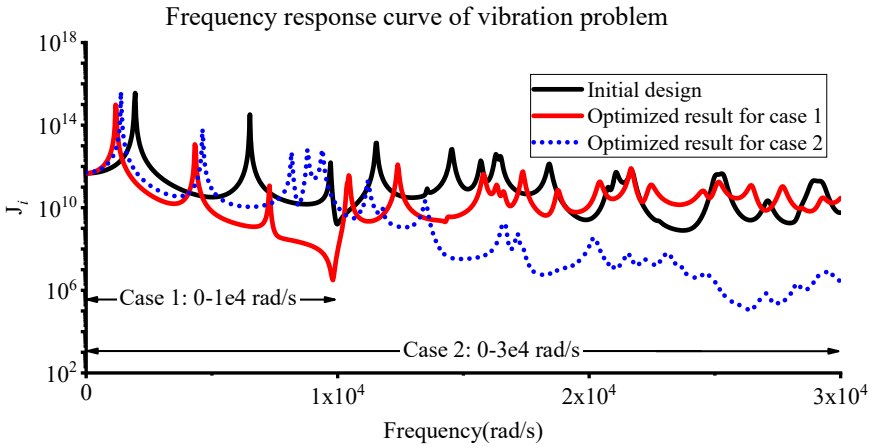

Fig. 13 Frequency response of the objective function for the optimized designs for the vibration suppression problem in Fig. 12.

For case 1, the optimized designs using the different ROMs with a varying number of basis vectors are listed in Table 3. When the number of basis vectors is small, such as 5 or 10, the optimization results differ drastically from the reference solution, and the objective function values predicted by the ROMs are not accurate. When enough basis vectors are included, the objective function values computed by the ROMs become accurate, and the ROMs demonstrate the ability to provide similar optimized material layouts as that of the full model. We then use the four ROMs (with N=70) to analyze the full model's optimized design and the relative errors (equation (28)) are presented in Fig. 14. The results confirm the previous observations, i.e. that solving the state equation yields accurate solutions for all methods, with SOMMG and SOAR yielding the most precision solutions. However, when solving the adjoint equation, the QSRV leads to errors in the high-frequency range that are much larger than $\varepsilon = 0.01$, some close to 100%. This is assumed to lead to the observed deviations in the optimized material layout.

Case 2 concerns a much wider frequency range and therefore covers more high-frequency components. As was seen in the previous sections, the ROMs had the most problems in capturing the high-frequency response, and hence, this optimization problem is expected to be very sensitive to numerical errors. The optimized designs are collected in Table 4 and from a qualitative inspection, it is clear that the QSRV fails to find a solution with a similar material layout as the full problem. On the other hand, the three second-order Krylov methods are found to yield similar results to that of the reference solution when a sufficient number of basis vectors is included. Again it is found that the QSRV provides an accurate evaluation of the objective function, but fails to solve the optimization problem due to the inaccurate determination of the adjoint vectors as shown in Fig. 11. For the other ROMs, especially SOMMG and SOAR, the relative errors of the adjoint solution satisfy $\varepsilon < 0.1$ for all frequency points. Even though the material layouts are not perfectly in tune with the full model, it is deemed that these methods can lead to satisfactory results.

a)

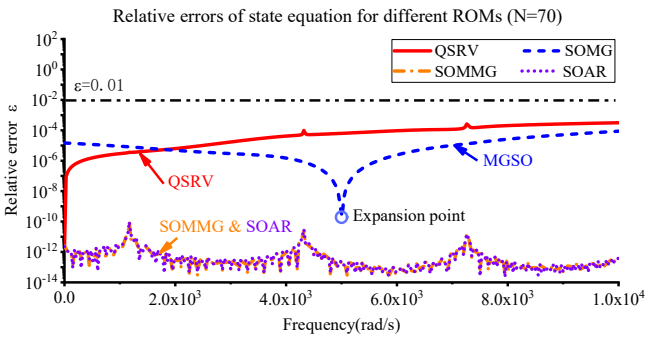

b)

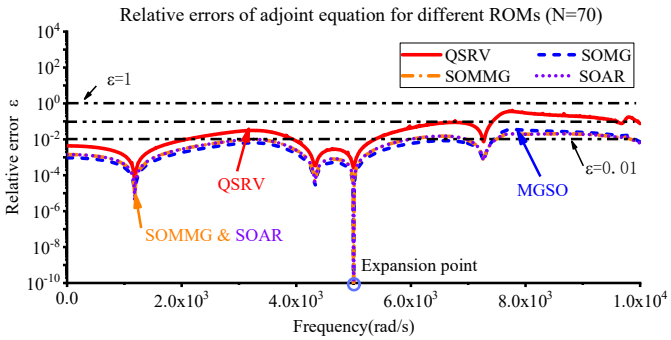

Fig. 14 Relative errors of the full solution in solving Case 1: a) the state equation, b) adjoint equation (*N*=70, vibration problem)

a)

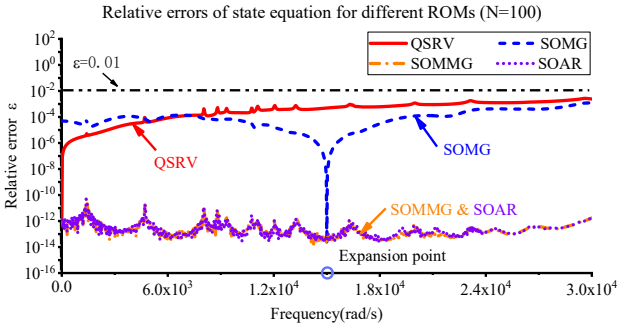

b)

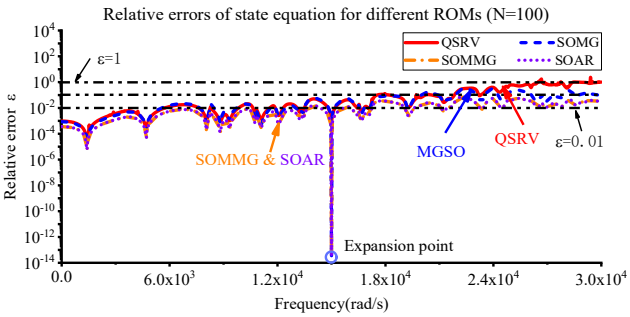

Fig. 15 Relative errors of the full solution in solving Case 2: a) the state equation, b) adjoint equation (*N*=100, vibration problem)

4.2.5 Single material topology optimization design

In this section, the ROMs are applied to a single material topology optimization design problem. The design domain is the same as given in section 4.2.3, yet only using material 1 and void. Here we suggest using the robust formulation to solve the single material problems to obtain stable convergence and clear solutions. The used topology optimization model is formulated as:

$$
\begin{aligned}
&\min_{\rho_e} && \max\left(J^i, J^d, J^e\right), && J = \sum_i^{N_f} \log_{10}\left(\frac{\left|\mathbf{FU}\left(\omega_i\right)\right|}{N_l}\right) \\
&s.t. && \sum_{e=1}^{N_e} \bar{\tilde{\rho}}_e^{(i)} v_e \Big/ V - V^* \le 0 \\
& && \mathbf{S}\left(\bar{\tilde{\rho}}_e^{(i,d,e)}, \omega_i\right)\mathbf{U}^{(i,d,e)}\left(\omega_i\right) = \mathbf{F}, \quad (i = 1, \ldots, N_f) \\
& && 0 \le \rho_e \le 1, \quad (e = 1, \ldots, N_e) \\
& && \log_{10}\left(\mathbf{U}^{(i)^{\mathrm{T}}}(0)\mathbf{K}\mathbf{U}^{(i)}(0)\right) \le \bar{C}
\end{aligned}
\tag{31}
$$

where superscripts *i*, *d*, *e* denote the intermediate, dilated, and eroded physical fields, respectively. The readers may refer to Ref. [67] for a detailed description of the robust formulation. It should be noted that, for single material problems, a static compliance constraint should be added to ensure a prescribed minimum stiffness. $\bar{C}$=19.5 is employed here. The optimization parameters, including filter radius, projection parameter η, and steepness parameter β are the same as those given in 4.2.3. $\eta\Delta$ used in the robust formulation is set to 0.25. The considered frequency band is [4e3, 1e4] rad/s and discretized by 201 frequency points. The results for different ROMs with different basis vectors are shown in Table 5. These results further validate the effectiveness of the ROMs and the better performances of SOAR and SOMMG.

4.2.6 Brief summary

Based on the numerical experiments regarding the solutions to the state equation and the adjoint equation together with the comparison of the optimized designs, the following intermediary conclusions can be made. First, the four projection-based ROMs (QSRV, SOGM, SOMMG, and SOAR) can yield accurate approximations covering a larger frequency range than the explicit Padé approximant. Due to the numerical error, QSRV_D and Padé expansion can solve the frequency problem only in a narrow frequency range and are not suitable for solving the wide range problem. Second, the second-order Krylov based methods (SOMG, SOMMG, and SOAR) perform much better than QSRV in solving the adjoint equation, including bandwidth and relative error. Third, the precision of SOMMG and SOAR are higher than SOMG, which validates the importance of the orthonormalization process. In the end, QSRV can solve a topology optimization problem in a relatively low frequency range, while SOMG, SOMMG, and SOAR are applicable for high frequency ranges.

Table 3 Case 1: Optimzed designs for the frequency interval [0, 1e4] rad/s obtained by different ROMs (vibration problem)

Full model: 7.8828

N	QSRV	SOMG	SOMMG	SOAR
5	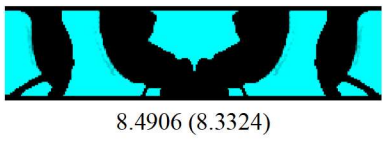 8.4906 (8.3324)	 8.1244 (7.9319)	 8.2731 (8.0206)	 8.3874 (8.1862)
10	 7.9341 (7.9281)	 7.9525 (7.9473)	 7.8523 (7.8524)	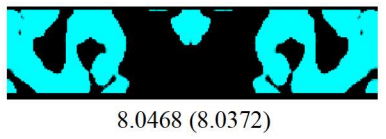 8.0468 (8.0372)
30	 **7.8943 (7.8943)**	 7.9005 (7.9005)	 7.9053 (7.9053)	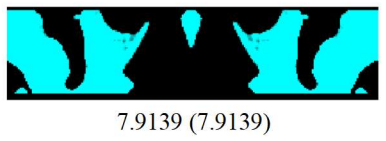 7.9139 (7.9139)
50	 7.9039 (7.9039)	 7.9054 (7.9054)	 7.8942 (7.8942)	 7.8903 (7.8903)
70	 7.9031 (7.9031)	 7.8998 (7.8998)	 **7.8830 (7.8830)**	 **7.8852 (7.8852)**
90	 7.9103 (7.9103)	 **7.8853 (7.8853)**	 7.8883 (7.8883)	 7.8906 (7.8906)
300	 7.9030 (7.9030)	 7.8892 (7.8892)	 7.8956 (7.8956)	 7.8885 (7.8885)

Note: 1. The first number below the result is recomputed used the full model, and the number in the parentheses is obtained by the ROM.

2. N represents the number of basis vectors for both the state equations and adjoint solutions.

Table 4 Case 2: Optimzed designs for the frequency interval [0, 3e4] rad/s obtained by different ROMs (vibration problem)

Full model: 6.2881

N	QSRV	SOMG	SOMMG	SOAR
10	 7.3486 (6.1913)	 7.3092 (6.8450)	 7.4797 (6.4884)	 7.4811 (6.2881)
40	 6.9372 (6.9324)	 6.5011 (6.5115)	 6.5687 (7.5602)	 6.6101 (6.6155)
70	 6.7501 (6.7500)	 6.3072 (6.3074)	 6.1938 (6.1938)	 6.2315 (6.2315)
100	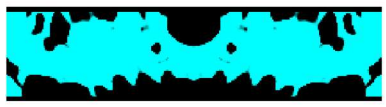 6.6702 (6.6701)	 6.2483 (6.2482)	 6.2705 (6.2705)	 6.2862 (6.2862)
130	 6.7302 (6.7302)	 6.2671 (6.2673)	 6.1965 (6.1965)	 6.2591 (6.2591)
150	 6.9847 (6.9847)	 6.3046 (6.3047)	 6.3496 (6.3496)	 6.3034 (6.3034)
300	 6.9354 (6.9354)	 6.4565 (6.4565)	 6.4106 (6.4106)	 6.3683 (6.3683)

Note: 1. The first number below the result is recomputed used the full model, and the number in the parentheses is obtained by the ROM.

2. N represents the number of basis vectors for both the state equations and adjoint solutions.

Table 5 Optimized designs for the frequency interval [4e3, 10e3] rad/s obtained by different ROMs (vibration problem, single material).

Full model: 12.7288

N	QSRV	SOMG	SOMMG	SOAR
5	 17.8036 (17.8061)	 17.7423(17.7536)	 17.7423(17.7436)	 17.7397(17.7514)
10	 17.7772(17.7726)	 19.0313(17.732)	 17.7332(17.7237)	 17.737(17.7357)
20	 17.7353(17.7353)	 17.7300(17.7300)	 17.7303(17.7303)	 17.7329(17.7328)
30	 17.7407(17.7407)	 17.7316(17.7316)	 17.7316(17.7316)	 17.7295(17.7295)
50	 17.7314(17.7314)	 17.7296(17.7296)	 17.7299(17.7299)	 17.7297(17.7297)
70	 17.7294(17.7294)	 17.7293(17.7293)	 17.7293(17.7293)	 17.7295(17.7295)

Note: 1. The first number below the result is recomputed used the full model, and the number in the parentheses is obtained by the ROM.

2. N represents the number of basis vectors for both the state equations and adjoint solutions.

3. Only material 1 is applied in this case.

4.3 Example 2: wave propagation problem

The second model problem concerns scalar out-of-plane shear wave propagation and is inspired by an example from Ref. [68]. In this case, the scalar wave equation written as

$$\rho\omega^2 w+\frac{\partial}{\partial x}\left(\mu\frac{\partial w}{\partial x}\right)+\frac{\partial}{\partial y}\left(\mu\frac{\partial w}{\partial y}\right)=0 \tag{32}$$

where ρ is the material density, w is the out-plane displacement, and μ is the shear modulus. The model problem is solved for the structure presented in Fig. 16 consisting of a square domain with size 0.12 m $\times$0.12 m, discretized by 60$\times$60 elements. As shown in Fig. 16a, the left edge is subjected to forced vibrations, and both left and right edges are modeled using a first-order absorbing boundary condition, i.e.,

$$\frac{\partial w}{\partial \mathbf{n}}+\frac{i\omega}{c}w=0 \tag{33}$$

where $\boldsymbol{n}$ represents the outward-pointing normal vector and $c=\sqrt{\mu/\rho}$ is the local shear wave speed. Note that the absorbing boundary conditions will contribute to the system damping. The amplitude of the force is 1e8N. The top and bottom edges are free boundaries given by the following Neumann type boundary condition

$$\mu\frac{\partial w}{\partial \mathbf{n}}=0 \tag{34}$$

The structural topology for the model problem consists of a grid of alternating phase 1 and phase 2 materials corresponding to Bragg gratings. For this topology, a large band-gap exists around the excitation frequency of 25e4 rad/s. The material properties of the two materials are listed in Table 6 and the considered frequency range is $\omega\in[1e4,\ 100e4]$ rad/s. The objective function and adjoint equation are evaluated at the dashed red line.

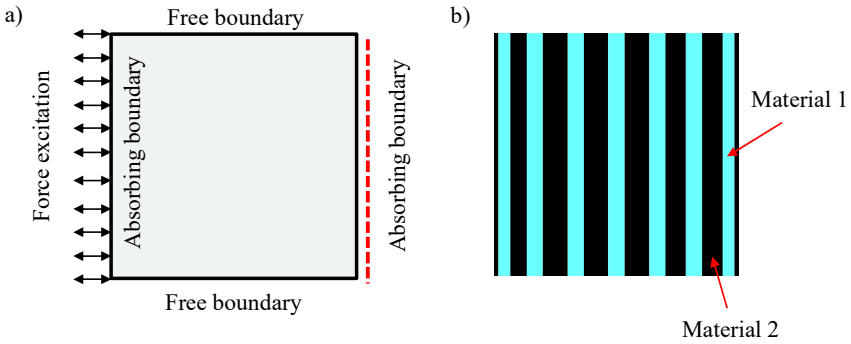

Fig. 16 The wave propagation test problem: (a) structural domain and boundary conditions; (b) structural topology used to evaluate the performance of the different ROMs.

Table 6 The material properties for the test problem 2

Material	Density (kg/m^3)	Modulus (GPa)	Poisson ratio	α_e	β_e
Material 1	1000	4	0.34	0	0
Material 2	2080	20	0.34	0	0

4.3.1 Solving the state equation

First, the state equation is solved by the different ROMs, including QSRV, SOMG, SOMMG and SOAR. The frequency response is presented in Fig. 17 using 50 basis vectors for each of the ROMs. From the frequency response plot, it is seen that the QSRV only yields a good approximation within a very narrow band. This is mainly attributed to the fact that the QSRV method does not include the damping matrix for generating the basis and hence, it cannot capture modes associated with wave propagation. However, it is also seen that none of the presented results in Fig. 13 are capable of fully resolving the entire frequency band. Therefore the number of included basis vectors is increased to N=150 and the relative error for the different ROMs are presented in Fig. 18. From these graphs, it is clear that the SOMMG and the SOAR work the best and that QSRV is the worst, with SOMG lying somewhere in the middle.

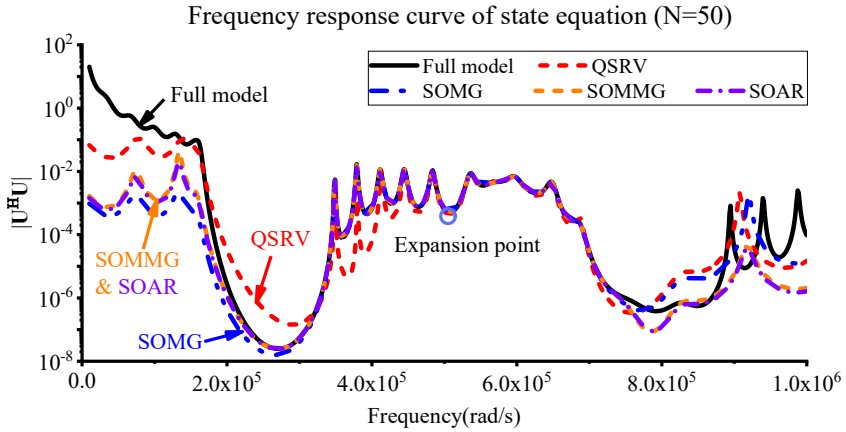

Fig. 17 The frequency response of the state equation (N=50, wave propagation problem).

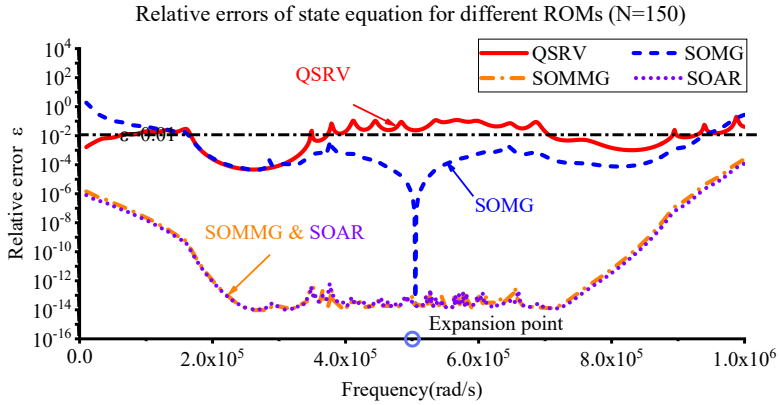

Fig. 18 Relative errors for solving the state equation (N=150, wave propagation problem).

Fig. 19 shows how the width of the sufficiently accurate frequency range changes as the number of basis vectors is increased. The plot demonstrates that the second-order Krylov based methods (SOMG, SOMMG, and SOAR) perform better than the QSRV method. Furthermore, and thanks to the introduction of correction factors in the orthonormalization process, the SOMMG and SOAR yield a wider bandwidth than SOMG, especially when a large number of basis vectors is used. The difference in the accuracy of the different ROMs is much more pronounced for this model problem than was the case for the first test problem. This is attributed to the fact that for this test case, the vibration modes are not confined to being standing waves and that the wave propagation is introduced to the model through the absorbing boundary condition. Since the QSRV method ignores damping in its construction, it is poorer in capturing the physics and needs many more basis

vectors to produce adequate results. This is contrary to the second-order Krylov methods, which include damping in their construction and thus are much better at capturing the physics. Finally, it is once again observed how the correction terms in the orthonormalization process for SOMMG and SOAR lead to superior numerical performance.

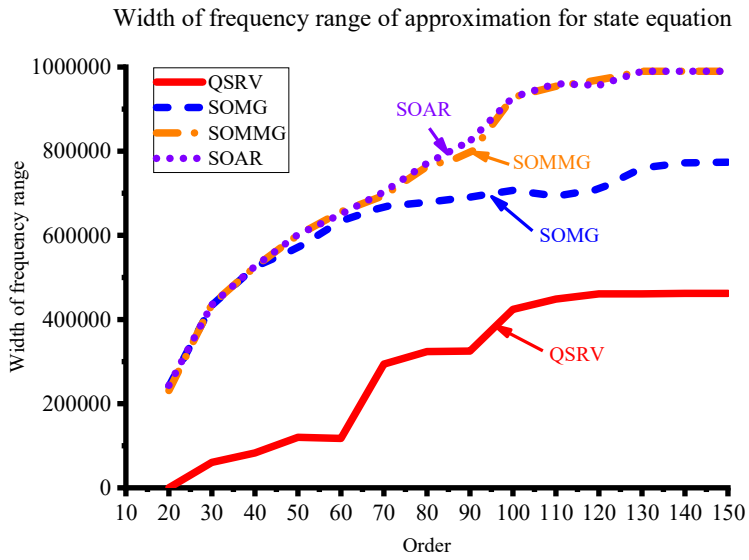

Fig. 19 Width of the frequency range as a function of the number of basis vectors for different ROMs when solving the state equation (wave propagation problem).

4.3.2 Solving the adjoint equation

The four ROMs are then used to solve the adjoint equation and the results are shown in Fig. 20 using 50 basis vectors. The results show that the ROMs can capture the frequency response near the expansion point for all tested methods. However, by comparing the relative errors of the different ROMs with N=150, as presented in Fig. 21, it is clear that none of the methods are capable of capturing the adjoint response for all considered frequencies. Again, this could be remedied by introducing a multi-point expansion strategy.

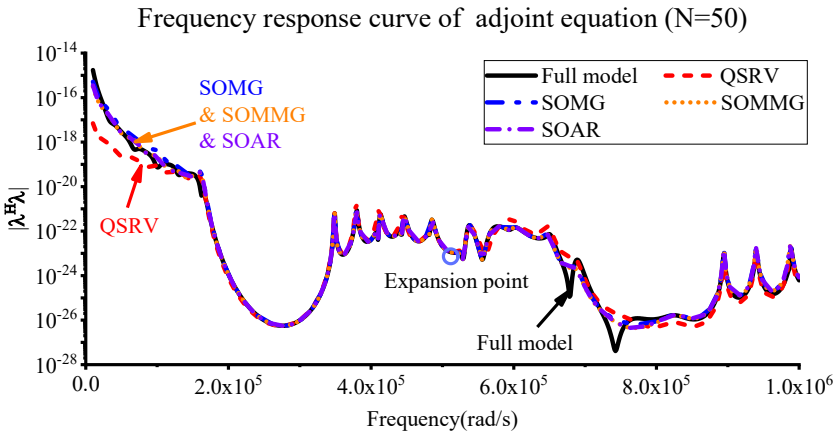

Fig. 20 The frequency response of the adjoint equation (N=50, wave propagation problem).

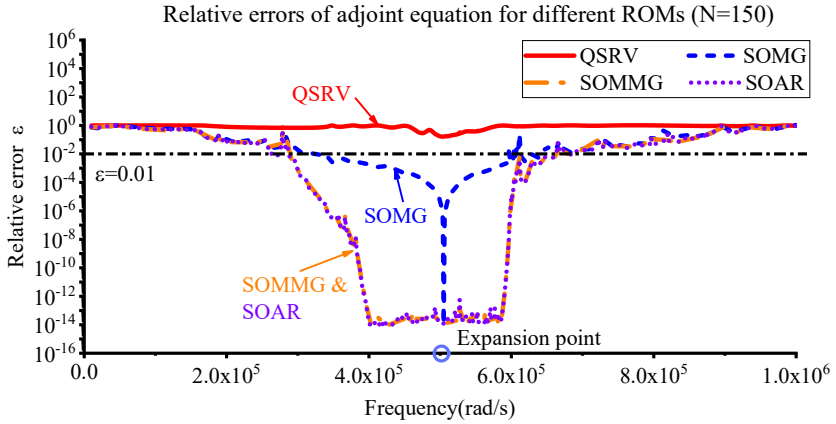

Fig. 21 Relative errors of solving the adjoint equation with N=150 (wave propagation problem).

The frequency width curves as a function of the number of basis vectors are presented in Fig. 22, which further confirms that the second-order Krylov methods (SOMG, SOMMG, and SOAR) provide improved results when the number of basis vectors is increased. At the same time, Fig. 22 shows a completely flat evolution for QSRV, indicating that the method is a poor choice for this specific model problem.

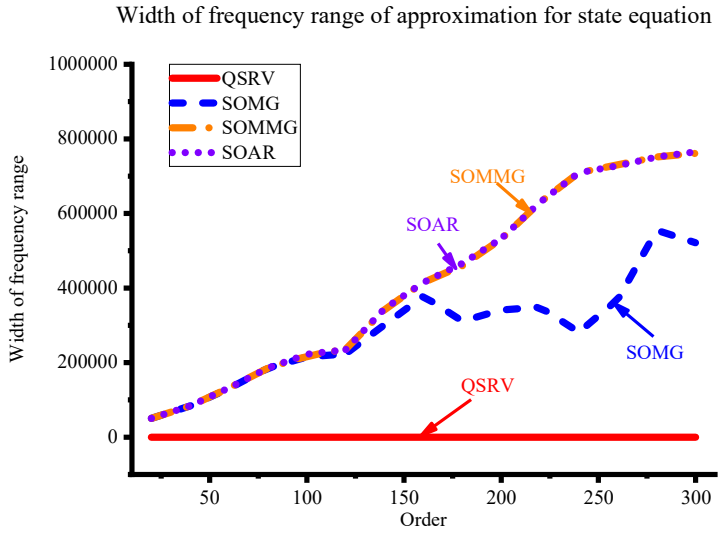

Fig. 22 Width of the frequency range as a function of the number of basis vectors for different ROMs when solving the adjoint equation (wave propagation problem).

Finally, we examine whether or not the basis vectors computed for the state equation can be reused for solving the adjoint equation. To this end, two analyses are conducted using the different number of basis vectors and for each of them, one is solved using the basis constructed for the state problem ("Reused"), whereas the other is solved using newly constructed basis vectors for the adjoint equation ("New basis"). The relative errors are shown in Fig. 23, from which it is obvious that directly using the basis vectors from the state equation causes large errors in the adjoint solutions regardless of the number of basis vectors included.

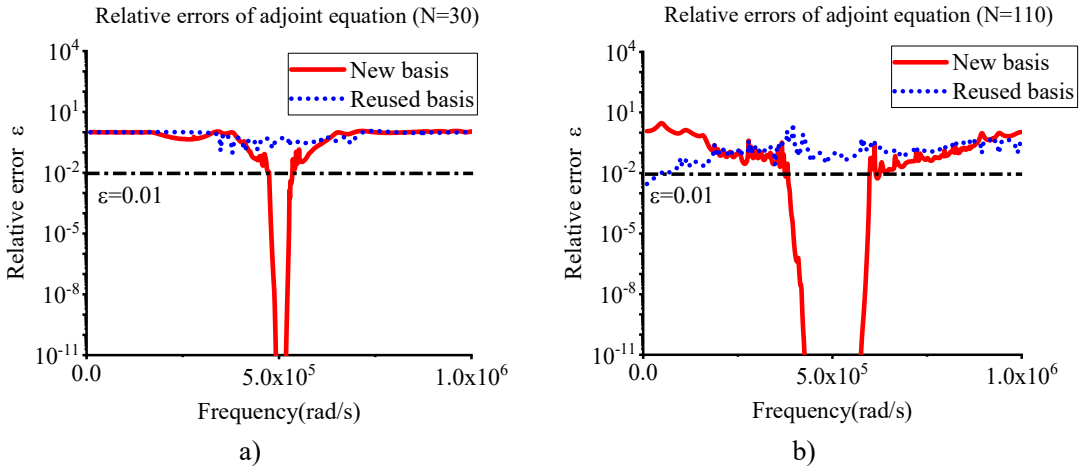

Fig. 23 Relative errors of solving the adjoint equation using the basis vectors for state equation or recomputed: a) N=30, b) N=110

4.3.3 Topology optimization results

In this section, optimized designs for the wave propagation problem are presented for which the objective is to maximize the vibration amplitude at the dashed red line on the right boundary, as shown in Fig. 24. The material properties are given in Table 6 but with an additional structural damping coefficient $\alpha_e = 1.25e4$ added. The design domain is discretized by 120×120 elements and a filter radius of 5.2 times the element size is used. A Heaviside projection filter is included and the continuation is the same as for example 1. Likewise, two frequency intervals are studied which are $\omega \in$ [1e4, 2e5] rad/s and $\omega \in$ [1e4, 4e5] rad/s, respectively. Both of these two cases are discretized by 401 frequency points. The optimized designs for the two cases are listed in Table 7 and Table 8, respectively, and the frequency responses for the optimized design, obtained by the full model, is presented in Fig. 25.

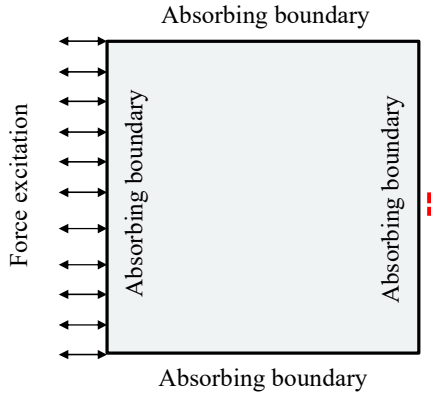

Fig. 24 Illustration of the design domain (the wave propagation problem).

From the results, we find that in both cases, QSRV fails to solve the optimization problems, even though 300 basis vectors are applied. The predicted objective values are not accurate, and the optimized material layout differs from the reference solution. The relative errors of the two cases are plotted in Fig. 26 and Fig. 27, respectively, from which we observe that QSRV fails to give an accurate approximation in solving the state and adjoint equations. Another difference between this example and example 1 is that, compared to SOMMG and SOAR, much more basis vectors are required in SOMG to obtain a satisfactory optimization solution. For example, in case 1, more than 110 basis vectors are required for obtaining an optimized result whose objective is near the reference

solution, while only 30 basis vectors are required for SOMMG and SOAR. Furthermore, even though the objective values of SOMG are similar to the reference, the material layout in the optimized results has a big deviation from the reference solutions. This can be explained through Fig. 26 and Fig. 27, which show that the relative errors of SOMG are much larger than SOMMG and SOAR.

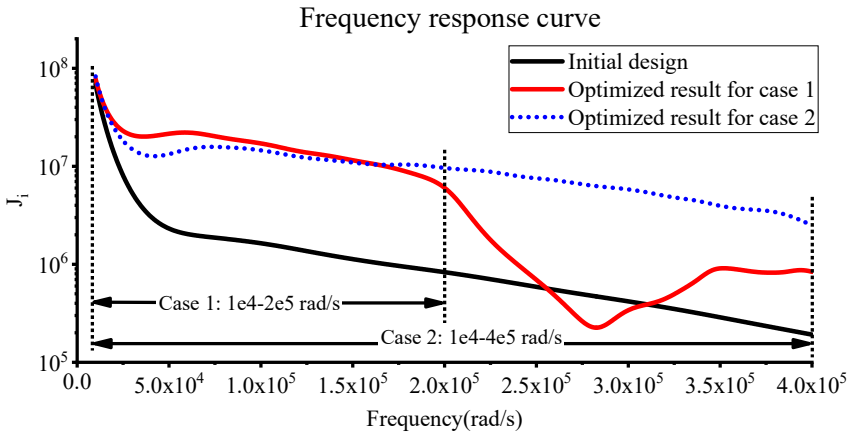

Fig. 25 The frequency response curves for the optimized results

a)

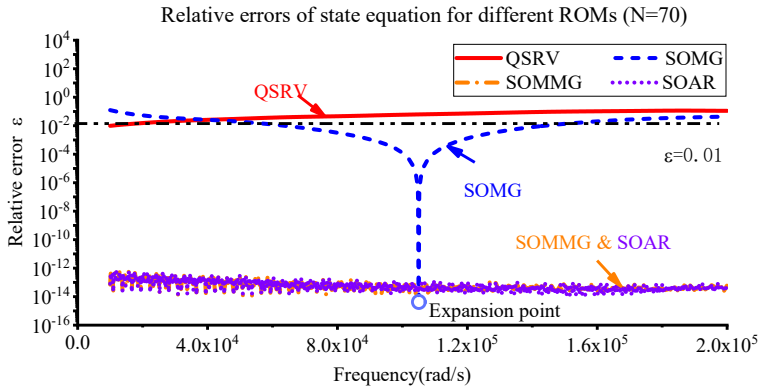

b)

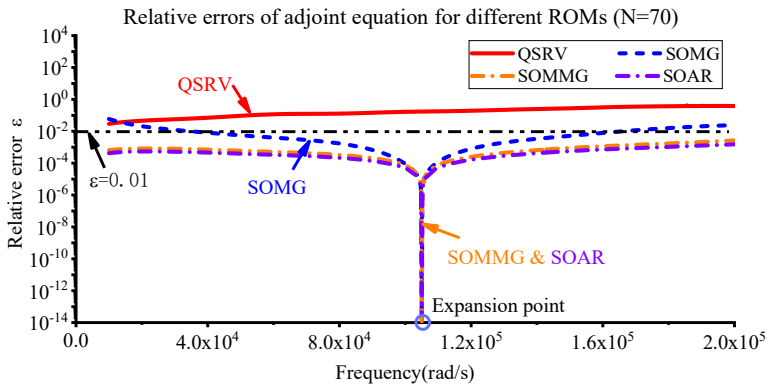

Fig. 26 Relative errors of the full solutions in solving Case 1: a) the state equation, b) adjoint equation (N=70)

a)

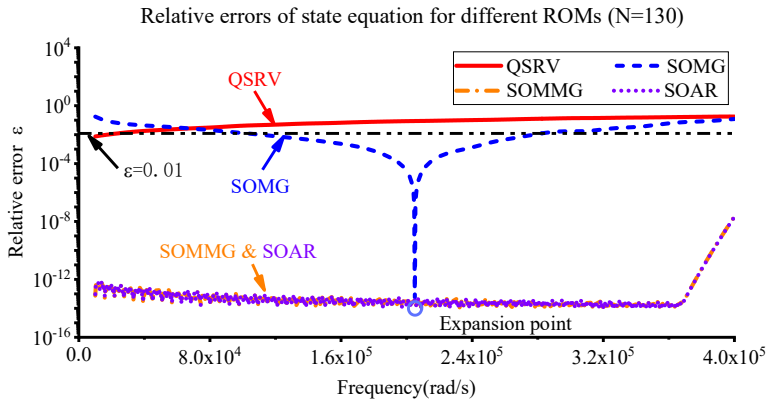

b)

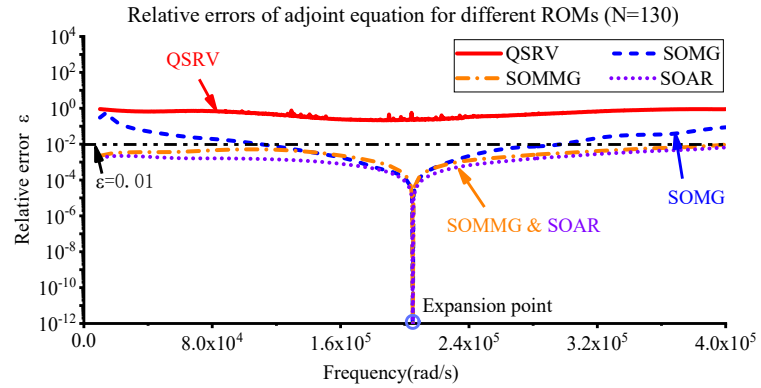

Fig. 27 Relative errors of the full solutions in solving Case 2: a) the state equation, b) adjoint equation (N=130)

4.3.4 Brief summary

Based on the numerical experiments in this example some conclusions can be made. First, for the wave propagation problem, QSRV cannot be applied since it fails to approximate the solutions for both the state and adjoint equations. Second, SOMMG and SOAR show great improvements compared to SOMG, not only in the precision but also in the bandwidth, many more basis vectors are needed in SOMG for solving a considered frequency range.

In this wave propagation example, we also find that the basis vectors computed for the state equation cannot be reused for solving the adjoint equation anymore and new basis vectors should be constructed for the adjoint equation. A computational cost analysis is also given, and a significant improvement in the computational efficiency can be obtained by using the ROMs.

Table 7 The material properties for the test problem 2: 1e4-2e5 rad/s

Full model	**: 788. 2819**	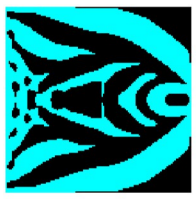

N	**70**	**90**	**110**	**130**	**180**	**250**	**300**
QSRV	 772.791 (775.5550)	 771.989 (773.991)	 773.526 (774.493)	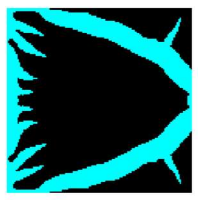 772.613 (774.601)	 779.498 (779.040)	 779.159 (778.994)	 779.365 (787.885)
SOMG	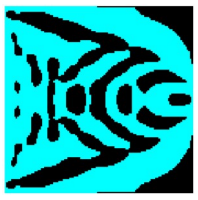 784.945 (791.594)	 787.491 (786.516)	 787.958 (785.677)	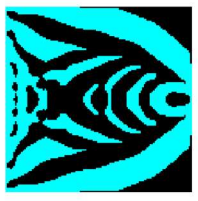 788.032 (786.472)	 788.059 (787.407)	 788.106 (788.584)	 788.084 (787.991)

N	**5**	**10**	**20**	**30**	**50**	**70**	**300**
SOMMG	 777.526 (781.126)	 782.180 (785.274)	 788.237 (788.306)	 788.231 (788.231)	 788.219 (788.219)	 788.514 (788.514)	 788.105 (788.105)
SOAR	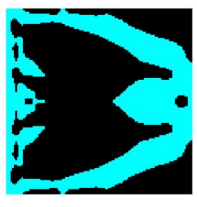 715.098 (772.975)	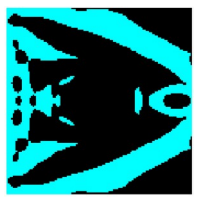 779.362 (785.016)	 788.113 (788.151)	 788.423 (788.423)	 788.081 (788.081)	 788.412 (788.412)	 788.424 (788.424)

Note: 1. The first number below the result is recomputed used the full model, and the number in the parentheses is obtained by the ROM.

2. N represents the number of basis vectors for both the state equations and adjoint solutions.

Table 8 The material properties for the test problem 2: 1e4-4e5 rad/s

Full model	**763.482**	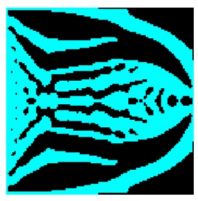

N	90	110	130	150	210	250	300
QSRV				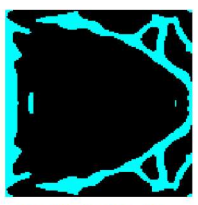	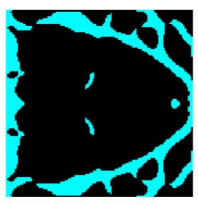	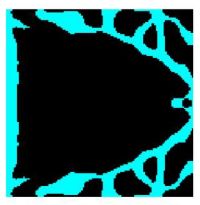	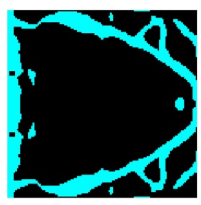
	719.557 (727.714)	723.419 (728.195)	725.127 (728.253)	721.891 (726.851)	724.801 (727.115)	726.417 (725.972)	**729.987 (730.213)**
SOMG	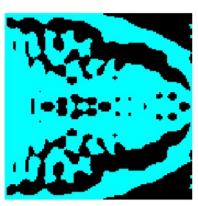	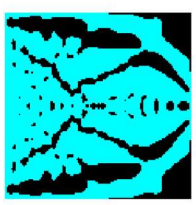	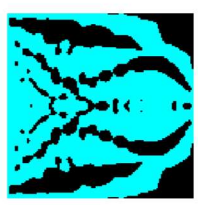	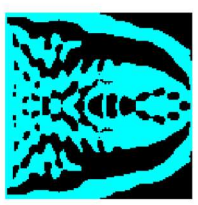	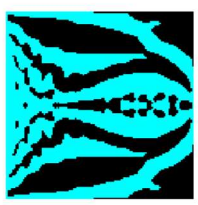	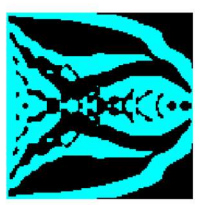	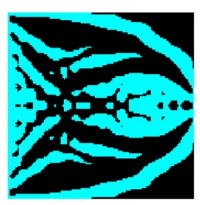
	751.015 (749.232)	756.623 (759.578)	757.871 (765.734)	758.418 (758.754)	761.761 (761.412)	762.589 (760.968)	**762.711 (762.203)**

N	30	50	70	90	110	130	300
SOMMG		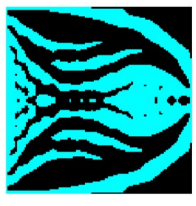	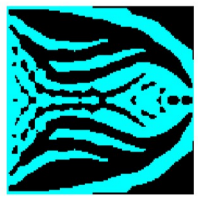		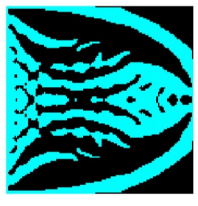	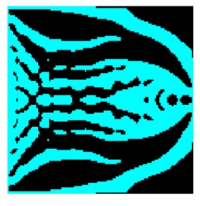	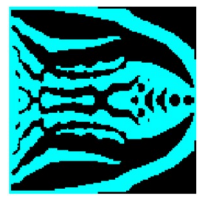
	754.466 (749.092)	762.618 (762.728)	**763.573 (763.581)**	762.877 (762.877)	762.962 (762.962)	763.121 (763.121)	763.395 (763.395)
SOAR	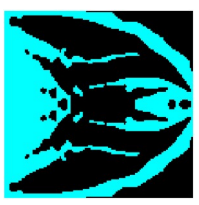	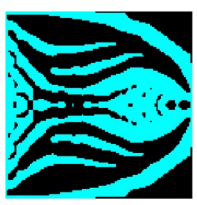	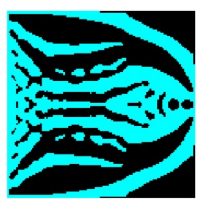	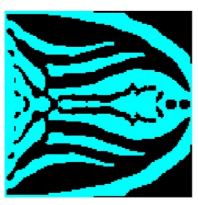	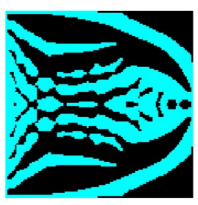	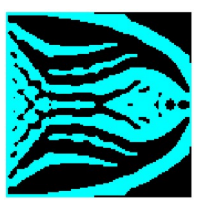	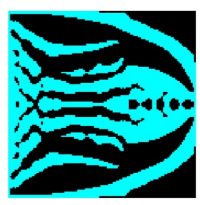
	756.091 (741.811)	763.084 (762.433)	763.383 (763.392)	**763.465 (764.066)**	763.223 (763.223)	763.221 (763.221)	762.937 (762.937)

Note: 1. The first number below the result is recomputed used the full model, and the number in the parentheses is obtained by the ROM.

2. N represents the number of basis vectors for both the state equations and adjoint solutions.

5 Summary and advice for future use

In this paper, a systematic comparative study of several ROMs for solving frequency problems is provided, including QSRV and QSRV_D methods, Padé expansion, and three second-order Krylov subspace methods (SOMG, SOMMG, and SOAR). Both the accuracy of the approximation of state and adjoint equations and the applicability to topology optimization problems are studied using the full model and above-mentioned ROMs in a wide-band frequency range. Two test problems, including a vibration problem and a wave propagation problem, are solved, analyzed, and compared. Based on the extensive numerical results, we come to the following conclusions. First, due to the numerical error, QSRV_D and Padé expansion can solve the frequency problem in a narrow frequency range only and are not suitable for solving the broadband problem. Second, the QSRV method shows excellent performance in solving the state equation of the vibration problem but fails to provide an accurate solution for the adjoint equation as well as for the wave propagation problem since damping is omitted from the construction of the reduced order basis. Third, the three second-order Krylov subspace methods (SOMG, SOMMG, and SOAR) solve the vibration problem, the wave propagation problem and all adjoint problems efficiently and accurately. However, the SOMG method needs many more basis vectors than SOMMG and SOAR to solve the wave propagation problem. Besides, SOMMG and SOAR have higher precision than SOMG, which validates the importance of the orthonormalization processes.

In future application of ROMs in frequency response topology optimization, SOAR and SOMMG are suggested for their superior accuracy and stability for solving both state and adjoint equations. However, if basis vectors computed for the state equation are reused for solving the adjoint equation it results in a significantly reduced accuracy. New basis vectors should therefore be constructed for the adjoint equation. If the frequency range is discretized into many frequency points, the computational cost can be significantly reduced using ROMs. For the 3D problems considered here, the reduction in computational time was in the order of 100-10000 compared to the full solution.

In continuing work, we study how to adaptively determine the number of basis vectors or the expansion points that should be used for providing a stable strategy in solving topology optimization problems. Another interesting future topic is combining the ROMs with high-performance computational methods, such as the multi-grid method or parallel computational method, to obtain frequency responses of large-scale problems.

Acknowledgments

Quhao Li acknowledges the financial support from the China Scholarship Council. Ole Sigmund and Niels Aage acknowledge the support from the Villum Foundation through the Villum Investigator Project InnoTop. This work is also supported by the National Natural Science Foundation of China (Grant No.11802164), Shandong Provincial Natural Science Foundation (Grant No. ZR2019BEE005), and the project funded by China Postdoctoral Science Foundation (2019M652375).

Reference

(1) Asua, E.; Etxebarria, V.; Feutchwanger, J.; Portilla, J. High-precision displacement sensor based on resonant cavities through an electronic interface based on Arduino. *Sensors and Actuators A: Physical* **2019**, *295*, 296-301.

(2) Zheng, Q.; Shi, B.; Li, Z.; Wang, Z. L. Recent Progress on Piezoelectric and Triboelectric Energy Harvesters in Biomedical Systems. *Advanced Science* **2017**, *4*, 1700029.

(3) Bendsøe, M. P.; Kikuchi, N. Generating optimal topologies in structural design using a homogenization method. *Computer Methods in Applied Mechanics and Engineering* **1988**, *71*, 197-224.

(4) Bendsøe, M. P. Optimal shape design as a material distribution problem. *Structural Optimization* **1989**, *1*, 193-202.

(5) Zhou, M.; Rozvany, G. The COC algorithm, Part II: Topological, geometrical and generalized shape optimization. *Computer Methods in Applied Mechanics and Engineering* **1991**, *89*, 309-336.

(6) Wang, M. Y.; Wang, X.; Guo, D. A level set method for structural topology optimization. *Computer methods in applied mechanics and engineering* **2003**, *192*, 227-246.

(7) Allaire, G.; Jouve, F.; Toader, A.-M. Structural optimization using sensitivity analysis and a level-set method. *Journal of Computational Physics* **2004**, *194*, 363-393.

(8) Xie, Y.; Steven, G. P. A simple evolutionary procedure for structural optimization. *Comput Struct* **1993**, *49*, 885-896.

(9) Guo, X.; Zhang, W.; Zhong, W. Doing topology optimization explicitly and geometrically—A new moving morphable components based framework. *Journal of Applied Mechanics* **2014**, *81*, 081009-081012.

(10) Zhou, Y.; Zhang, W.; Zhu, J.; Xu, Z. Feature-driven topology optimization method with signed distance function. *Computer Methods in Applied Mechanics and Engineering* **2016**, *310*, 1-32.

(11) Díaaz, A. R.; Kikuchi, N. Solutions to shape and topology eigenvalue optimization problems using a homogenization method. *International Journal for Numerical Methods in Engineering* **1992**, *35*, 1487-1502.

(12) Ma, Z.; Cheng, H.; Kikuchi, N. Structural design for obtaining desired eigenfrequencies by using the topology and shape optimization method. *Computing Systems in Engineering* **1994**, *5*, 77-89.

(13) Jensen, J. S.; Pedersen, N. L. On maximal eigenfrequency separation in two-material structures: the 1D and 2D scalar cases. *Journal of Sound and Vibration* **2006**, *289*, 967-986.

(14) Li, Q.; Wu, Q.; Liu, J.; He, J.; Liu, S. Topology optimization of vibrating structures with frequency band constraint. *Structural and Multidisciplinary Optimization* **2020**, 1-16.

(15) Dahl, J.; Jensen, J. S.; Sigmund, O. Topology optimization for transient wave propagation problems in one dimension. *Structural and Multidisciplinary Optimization* **2008**, *36*, 585-595.

(16) James, K. A.; Waisman, H. Topology optimization of viscoelastic structures using a time-dependent adjoint method. *Computer Methods in Applied Mechanics and Engineering* **2015**, *285*, 166-187.

(17) Wu, S.; Zhang, Y.; Liu, S. Topology optimization for minimizing the maximum temperature of transient heat conduction structure. *Structural and Multidisciplinary Optimization* **2019**, *60*, 69-82.

(18) Jog, C. S. TOPOLOGY DESIGN OF STRUCTURES SUBJECTED TO PERIODIC LOADING. *Journal of Sound and Vibration* **2002**, *253*, 687-709.

(19) Olhoff, N.; Du, J. Generalized incremental frequency method for topological designof continuum structures for minimum dynamic compliance subject to forced vibration at a prescribed low or high value of the excitation frequency. *Structural and Multidisciplinary Optimization* **2016**, *54*, 1113-1141.

(20) Long, K.; Wang, X.; Liu, H. Stress-constrained topology optimization of continuum structures subjected to harmonic force excitation using sequential quadratic programming. *Structural and Multidisciplinary Optimization* **2019**, *59*, 1747-1759.

(21) Tcherniak, D. Topology optimization of resonating structures using SIMP method. *International Journal for Numerical Methods in Engineering* **2002**, *54*, 1605-1622.

(22) Larsen, A. A.; Laksafoss, B.; Jensen, J. S.; Sigmund, O. Topological material layout in plates for vibration suppression and wave propagation control. *Structural and Multidisciplinary Optimization* **2009**, *37*, 585-594.

(23) Bonnecaze, R. T.; Rodin, G. J.; Sigmund, O.; Søndergaard Jensen, J. Systematic design of phononic band–gap materials and structures by topology optimization. *Philosophical Transactions of the Royal Society of London. Series A: Mathematical, Physical and Engineering Sciences* **2003**, *361*, 1001-1019.

(24) Matzen, R.; Jensen, J. S.; Sigmund, O. Topology optimization for transient response of photonic crystal structures. *J. Opt. Soc. Am. B* **2010**, *27*, 2040-2050.

(25) Nakshatrala, P. B.; Tortorelli, D. A. Topology optimization for effective energy propagation in rate-independent elastoplastic material systems. *Computer Methods in Applied Mechanics and Engineering* **2015**, *295*, 305-326.

(26) Kennedy, G. J.; Martins, J. R. R. A. A parallel finite-element framework for large-scale gradient-based design optimization of high-performance structures. *Finite Elements in Analysis and Design* **2014**, *87*, 56-73.

(27) Aage, N.; Lazarov, B. S. Parallel framework for topology optimization using the method of moving asymptotes. *Structural and multidisciplinary optimization* **2013**, *47*, 493-505.

(28) Amir, O.; Aage, N.; Lazarov, B. S. On multigrid-CG for efficient topology optimization. *Structural and Multidisciplinary Optimization* **2014**, *49*, 815-829.

(29) Kambampati, S.; Jauregui, C.; Museth, K.; Kim, H. A. Large-scale level set topology optimization for elasticity and heat conduction. *Structural and Multidisciplinary Optimization* **2020**, *61*, 19-38.

(30) Aage, N.; Andreassen, E.; Lazarov, B. S.; Sigmund, O. Giga-voxel computational morphogenesis for structural design. *Nature* **2017**, *550*, 84-86.

(31) Baandrup, M.; Sigmund, O.; Polk, H.; Aage, N. Closing the gap towards super-long suspension bridges using computational morphogenesis. *Nature Communications* **2020**, *11*, 2735.

(32) Ferrari, F.; Lazarov, B. S.; Sigmund, O. Eigenvalue topology optimization via efficient multilevel solution of the frequency response. *International Journal for Numerical Methods in Engineering* **2018**, *115*, 872-892.

(33) Ferrari, F.; Sigmund, O. Towards solving large-scale topology optimization problems with buckling constraints at the cost of linear analyses. *Computer Methods in Applied Mechanics and Engineering* **2020**, *363*, 112911.

(34) Ma, Z. D.; Kikuchi, N.; Hagiwara, I. Structural topology and shape optimization for a frequency response problem. *Computational Mechanics* **1993**, *13*, 157-174.

(35) Cornwell, R. E.; Craig Jr, R. R.; Johnson, C. P. On the application of the mode-acceleration method to structural engineering problems. *Earthquake Engineering & Structural Dynamics* **1983**, *11*, 679-688.

(36) Liu, H.; Zhang, W.; Gao, T. A comparative study of dynamic analysis methods for structural topology optimization under harmonic force excitations. *Structural and Multidisciplinary Optimization* **2015**, *51*, 1321-1333.

(37) Zhao, J.; Yoon, H.; Youn, B. D. An adaptive hybrid expansion method (AHEM) for efficient structural topology optimization under harmonic excitation. *Structural and Multidisciplinary Optimization* **2020**.

(38) Zhao, X.; Wu, B.; Li, Z.; Zhong, H. A method for topology optimization of structures under harmonic excitations. *Structural and Multidisciplinary Optimization* **2018**, *58*, 475-487.

(39) Kang, Z.; Zhang, X.; Jiang, S.; Cheng, G. J. S.; Optimization, M. On topology optimization of damping layer in shell structures under harmonic excitations. **2012**, *46*, 51-67.

(40) Kang, Z.; He, J.; Shi, L.; Miao, Z. A method using successive iteration of analysis and design for large-scale topology optimization considering eigenfrequencies. *Computer Methods in Applied Mechanics and Engineering* **2020**, *362*, 112847.

(41) Jensen, J. S. Topology optimization of dynamics problems with Padé approximants. *International Journal for Numerical Methods in Engineering* **2007**, *72*, 1605-1630.

(42) Yoon, G. H. Structural topology optimization for frequency response problem using model reduction schemes. *Computer Methods in Applied Mechanics and Engineering* **2010**, *199*, 1744-1763.

(43) Demmel, J. W.: *Applied numerical linear algebra*; SIAM, 1997.

(44) Bai, Z.; Demmel, J.; Dongarra, J.; Ruhe, A.; van der Vorst, H.: *Templates for the solution of algebraic eigenvalue problems: a practical guide*; SIAM, 2000.

(45) Sittl, C.; Marburg, S.; Wagner, M. Application of a Krylov subspace method for an efficient solution of acoustic transfer functions. *Mechanical Systems and Signal Processing* **2021**, *148*, 107135.

(46) Panagiotopoulos, D.; Deckers, E.; Desmet, W. Krylov subspaces recycling based model order reduction for acoustic BEM systems and an error estimator. *Computer Methods in Applied Mechanics and Engineering* **2020**, *359*, 112755.

(47) Hughes, T. J. R.: *The finite element method: linear static and dynamic finite element analysis*; Courier Corporation, 2012.

(48) Behbahani-Nejad, M.; Shekari, Y. The accuracy and efficiency of a reduced-order model for transient flow analysis in gas pipelines. *Journal of Petroleum Science and Engineering* **2010**, *73*, 13-19.

(49) Weickum, G.; Eldred, M. S.; Maute, K. A multi-point reduced-order modeling approach of transient structural dynamics with application to robust design optimization. *Structural and Multidisciplinary Optimization* **2008**, *38*, 599.

(50) Niu, B.; He, X.; Shan, Y.; Yang, R. On objective functions of minimizing the vibration response of continuum structures subjected to external harmonic excitation. *Structural and Multidisciplinary Optimization* **2018**, *57*, 2291-2307.

(51) Bendsøe, M. P.; Sigmund, O. Material interpolation schemes in topology optimization. *Archive of Applied Mechanics* **1999**, *69*, 635-654.

(52) Wang, F.; Lazarov, B. S.; Sigmund, O. On projection methods, convergence and robust formulations in topology optimization. *Structural and Multidisciplinary Optimization* **2010**, *43*, 767-784.

(53) Bendsøe, M. P.; Sigmund, O.: *Topology optimization: Theory methods and applications*; Springer-Verlag: Berlin, 2003.

(54) Li, L.; Hu, Y.; Wang, X.; Lü, L. A hybrid expansion method for frequency response functions of non-proportionally damped systems. *Mechanical Systems and Signal Processing* **2014**, *42*, 31-41.

(55) Qu, Z. Q. Hybrid expansion method for frequency responses and their sensitivities, part 1: undamped systems. *Journal of Sound and Vibration* **2000**, *231*, 175-193.

(56) Pillage, L. T.; Rohrer, R. A. Asymptotic waveform evaluation for timing analysis. *IEEE Transactions on Computer-Aided Design of Integrated Circuits and Systems* **1990**, *9*, 352-366.

(57) Hetmaniuk, U.; Tezaur, R.; Farhat, C. Review and assessment of interpolatory model order reduction methods for frequency response structural dynamics and acoustics problems. *International Journal for Numerical Methods in Engineering* **2012**, *90*, 1636-1662.

(58) Wilson, E. L.; Yuan, M.-W.; Dickens, J. M. Dynamic analysis by direct superposition of Ritz vectors. *Earthquake Engineering & Structural Dynamics* **1982**, *10*, 813-821.

(59) Léger, P. Load dependent subspace reduction methods for structural dynamic computations. *Computers & Structures* **1988**, *29*, 993-999.

(60) Gu, J.; Ma, Z.-D.; M. Hulbert, G. A new load-dependent Ritz vector method for structural dynamics analyses: quasi-static Ritz vectors. *Finite Elements in Analysis and Design* **2000**, *36*, 261-278.

(61) Hyun, J.; Kook, J.; Wang, S. Efficient and stable model reduction scheme for the numerical simulation of broadband acoustic metamaterials. *Computers & Mathematics with Applications* **2015**, *69*, 876-892.

(62) Slone, R. D. Fast frequency sweep model order reduction of polynomial matrix equations resulting from finite element discretizations. **2002**.

(63) Slone, R. D.; Lee, R.; Jin-Fa, L. Well-conditioned asymptotic waveform evaluation for finite elements. *IEEE Transactions on Antennas and Propagation* **2003**, *51*, 2442-2447.

(64) Bai, Z.; Su, Y. SOAR: A Second-order Arnoldi Method for the Solution of the Quadratic Eigenvalue Problem. *SIAM Journal on Matrix Analysis and Applications* **2005**, *26*, 640-659.

(65) Bai, Z.; Su, Y. Dimension Reduction of Large-Scale Second-Order Dynamical Systems via a Second-Order Arnoldi Method. *SIAM Journal on Scientific Computing* **2005**, *26*, 1692-1709.

(66) Xiao, M.; Lu, D.; Breitkopf, P.; Raghavan, B.; Dutta, S.; Zhang, W. J. S.; Optimization, M. On-the-fly model reduction for large-scale structural topology optimization using principal components analysis. **2020**, *62*, 209-230.

(67) Wang, F.; Lazarov, B. S.; Sigmund, O. On projection methods, convergence and robust formulations in topology optimization. *Structural and Multidisciplinary Optimization* **2011**, *43*, 767-784.

(68) Sigmund, O.; Søndergaard Jensen, J. Systematic design of phononic band–gap materials and structures by topology optimization. *Philosophical Transactions of the Royal Society of London. Series A: Mathematical, Physical and Engineering Sciences* **2003**, *361*, 1001-1019.